Article

Non-reciprocal phase transitions

https://doi.org/10.1038/s41586-021-03375-9

Received: 9 April 2020

Accepted: 19 February 2021

Published online: 14 April 2021

Check for updates

Michel Fruchart[1,5], Ryo Hanai[1,2,3,5], Peter B. Littlewood[1] & Vincenzo Vitelli[1,4]✉

Out of equilibrium, a lack of reciprocity is the rule rather than the exception. Non-reciprocity occurs, for instance, in active matter[1–6], non-equilibrium systems[7–9], networks of neurons[10,11], social groups with conformist and contrarian members[12], directional interface growth phenomena[13–15] and metamaterials[16–20]. Although wave propagation in non-reciprocal media has recently been closely studied[1,16–20], less is known about the consequences of non-reciprocity on the collective behaviour of many-body systems. Here we show that non-reciprocity leads to time-dependent phases in which spontaneously broken continuous symmetries are dynamically restored. We illustrate this mechanism with simple robotic demonstrations. The resulting phase transitions are controlled by spectral singularities called exceptional points[21]. We describe the emergence of these phases using insights from bifurcation theory[22,23] and non-Hermitian quantum mechanics[24,25]. Our approach captures non-reciprocal generalizations of three archetypal classes of self-organization out of equilibrium: synchronization, flocking and pattern formation. Collective phenomena in these systems range from active time-(quasi) crystals to exceptional-point-enforced pattern formation and hysteresis. Our work lays the foundation for a general theory of critical phenomena in systems whose dynamics is not governed by an optimization principle.

To explore how non-reciprocity affects phase transitions, consider multiple species or fields with asymmetric interactions that are modelled by vector order parameters $\mathbf{v}_a(t, \mathbf{x})$, for each species a. These can encode, for instance, the average velocities of self-propelled particles[26,27], the average phases of coupled oscillators or the amplitude and position of periodic patterns (Fig. 1a–d). The $\mathbf{v}_a(t, \mathbf{x})$ could either be distinct fields, or different harmonics of the same physical field, as in interface-growth experiments[13–15] (Fig. 1e, f). Systems with gain and loss[18,20,28–31] can also be mapped onto non-reciprocal systems.

All such systems are described by the evolution equation

$$\partial_t \mathbf{v}_a = \mathbb{A}_{ab}\mathbf{v}_b + \mathbb{B}_{abcd}\,(\mathbf{v}_b \cdot \mathbf{v}_c)\mathbf{v}_d + \mathcal{O}(\nabla), \tag{1}$$

where summation over repeated indices is implied. Equation (1) is (up to third order in $\mathbf{v}_a$) the most general dynamical system invariant under rotations. In flocking, rotational symmetry arises from the isotropy of space, whereas in synchronization and pattern formation it arises from time or space translation invariance. Different symmetries or other representations of rotations can be similarly enforced[22]; see Methods and Supplementary Information section XI. The quantities $\mathbb{A}_{ab}$ and $\mathbb{B}_{abcd}$ are arrays of parameters that couple different species. We have temporarily omitted in equation (1) terms that have spatial derivatives, represented by $\mathcal{O}(\nabla)$, but we have retained nonlinearities that are essential for discussing phase transitions. Here, we allow the macroscopic coefficients to be asymmetric, for example, $\mathbb{A}_{ab} \neq \mathbb{A}_{ba}$. For equilibrium phase transitions, these coefficients would be fully symmetric because the dynamics $\partial_t \mathbf{v}_a = -\partial_{\mathbf{v}_a} F$ is derived from a (free) energy F. Removing this constraint extends the theory of critical phenomena[32] to non-reciprocal systems.

Dynamical systems described by equation (1) arise in various forms of non-reciprocal matter. Consider, for instance, the Kuramoto model of synchronization[33]

$$\partial_t \theta_m = \omega_m + \sum_n J_{mn}\,\sin(\theta_n - \theta_m) + \eta(t), \tag{2}$$

which describes coupled oscillators m with phases $\theta_m(t)$, frequencies ω_m and couplings J_{mn}, and where $\eta(t)$ is a random noise. Equation (2) with $\omega_m = 0$ also captures the Vicsek model of flocking[34,35], with the oscillators replaced by self-propelled particles moving at constant speed v_0 in the planar direction θ_m. Their positions $\mathbf{r}_m$ follow

$$\partial_t \mathbf{r}_m = v_0 \begin{pmatrix} \cos\theta_m \\ \sin\theta_m \end{pmatrix}. \tag{3}$$

In both models, agent m tries to align (be in phase) with agent n when $J_{mn} > 0$, or to antialign when $J_{mn} < 0$. Above a critical coupling, both models exhibit a transition from incoherent motion (incoherent oscillations) to flocking (synchronization) heralded by a non-vanishing order parameter $\mathbf{v}_a$ (Fig. 1a, c). We now consider two populations with non-reciprocal interactions $J_{mn} \neq J_{nm}$ (refs. [2–6,8,10–12,36–39]). We show in Methods and Supplementary Information section V that coarse-graining these microscopic models leads to equation (1) with asymmetric coefficients and the addition of spatial derivative terms.

Equation (1), viewed as an amplitude equation, also describes non-reciprocal pattern formation (Fig. 1e). For example, the Swift–Hohenberg model[40],

$$\partial_t u_a = r_{ab}u_b - (1 + \nabla^2)^2 u_a - g u_a^3, \tag{4}$$

[1]James Franck Institute and Department of Physics, University of Chicago, Chicago, IL, USA. [2]Department of Physics, Osaka University, Toyonaka, Japan. [3]Pritzker School of Molecular Engineering, University of Chicago, Chicago, IL, USA. [4]Kadanoff Center for Theoretical Physics, University of Chicago, Chicago, IL, USA. [5]These authors contributed equally: Michel Fruchart, Ryo Hanai. ✉e-mail: vitelli@uchicago.edu

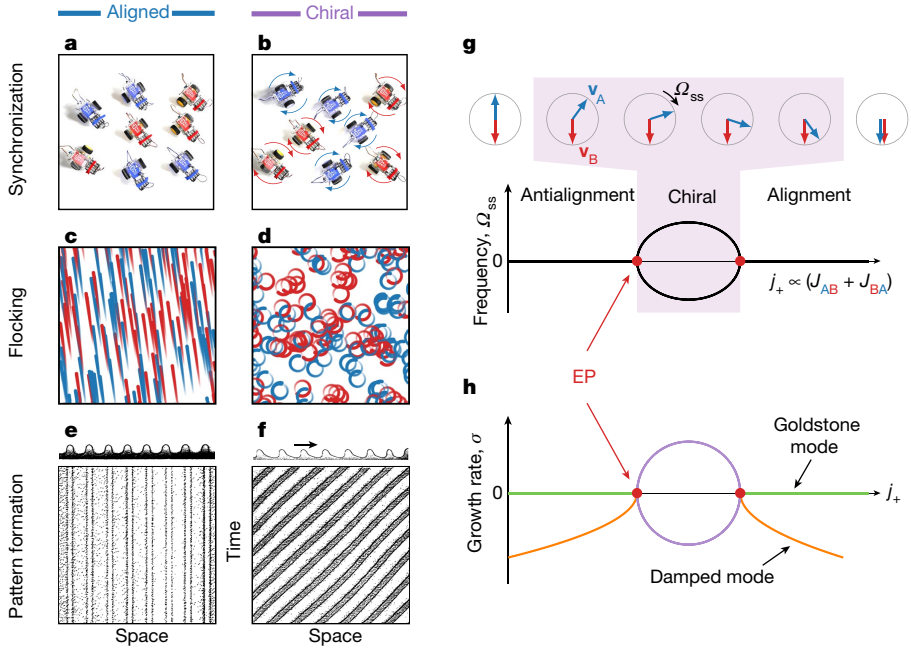

Fig. 1 | Exceptional transitions: examples and mechanism. Non-reciprocal interactions ($J_{AB} \neq J_{BA}$) between two species A and B (in blue and red) induce a phase transition from static alignment to a chiral motion that spontaneously breaks parity. **a**, **b**, Non-reciprocal synchronization. Robots (programmed as non-reciprocal spins) spontaneously rotate either clockwise or anticlockwise, despite no average natural frequency ($\omega_m = 0$ in equation (2)). (Methods, Supplementary Information sections IX, XIV, Supplementary Video 1) **c**, **d**, Non-reciprocal flocking. Self-propelled particles run in circles despite the absence of external torques (Supplementary Information sections V–VII and Supplementary Video 3). **e**, **f**, Non-reciprocal pattern formation. A one-dimensional pattern starts travelling, either to the left or to the right (Methods). The figure represents an experimental observation of viscous fingering at an oil–air interface adapted with permission from ref. [15], copyrighted by the American Physical Society. **g**, Schematic bifurcation diagram of the exceptional transition showing the frequency of the steady state, Ω_{ss}. Between the static (anti)aligned phases with $\Omega_{ss} = 0$, an intermediate chiral phase spontaneously breaks parity. Two equivalent steady states (clockwise and anticlockwise, corresponding to opposite values of Ω_{ss}) are present in this time-dependent phase, which can be seen as a manifestation of spontaneous PT-symmetry breaking. The chiral phase continuously interpolates between the antialigned and aligned phases, both through $|\Omega_{ss}|$ and through the angle between the order parameters $\mathbf{v}_A$ and $\mathbf{v}_B$. **h**, The transition between (anti)aligned and chiral phases occurs through the coalescence of a damped (orange) and a Goldstone (green) mode at an exceptional point (EP, red circle). In the chiral phase, the growth rates are drawn in purple.

with $r_{ab} \neq r_{ba}$, reduces to equation (1) by letting $u_a(x) = A_a(x)e^{ikx} + \text{c.c.}$, where k is a wavevector and the complex amplitude is decomposed as $A_a \equiv v_a^x + iv_a^y$ (Methods).

Let us start with two populations A and B, and parity not explicitly broken. When the interactions are reciprocal, we find (besides a disordered phase) two static phases where $\mathbf{v}_A$ and $\mathbf{v}_B$ (red and blue arrows in Fig. 1g) are (anti)aligned in analogy with (anti)ferromagnetism. When the interactions are non-reciprocal, the coefficients in equation (1) become asymmetric (for example, $\mathbb{A}_{ab} \neq \mathbb{A}_{ba}$) and a time-dependent chiral phase with no equilibrium analogue emerges between the static phases (Fig. 1g, h). In the chiral phase, parity is spontaneously broken: $\mathbf{v}_A$ and $\mathbf{v}_B$ rotate at a constant speed Ω_{ss} with a fixed relative angle, either clockwise or anticlockwise (see Supplementary Video 1 for a demonstration with programmable robots). Figure 1a–f illustrates the aligned–chiral transition in synchronization, flocking and pattern formation. This transition also occurs in viscous fingering[15,41] (Fig. 1e, f), liquid-crystal solidification[42], lamellar eutectics growth[43], overflowing fountains[44], and other natural phenomena that can be modelled by amplitude equations with asymmetric couplings between different harmonics of the same field (Methods).

The chiral phase is caused by the frustration experienced by agents with opposite goals: agent A wants to align with agent B but not vice-versa. This dynamical frustration results in a chase and runaway motion of the order parameters $\mathbf{v}_a$ (where $a = A, B$). Crucially, a stable chiral phase hinges on a subtle interplay between noise and many-body effects. Consider the exactly solvable bipartite Kuramoto model in equation (2) with $\eta(t) = 0$ and identical frequencies within each species. This system can be mapped to the dynamics of only two agents (Supplementary Information section IX). Unless $J_{AB} = -J_{BA}$ exactly, agents A and B would eventually catch up with each other and reach alignment or anti-alignment (henceforth, (anti)alignment) (Supplementary Information section VIII). However, frequency disorder or noise in equation (2) constantly resets the chiral motion of A/B pairs. The noise-activated motions of individual agents become macroscopically correlated through their interactions: the chiral phase is stabilized. We verified this by computing the standard deviations of the order parameters that decrease as $1/\sqrt{N}$ with the number of agents N; see Extended Data Fig. 2b. In flocking too, noise enlarges the chiral phase region (Fig. 2b, c).

Contrast our many-body chiral phase with parity-breaking phenomena occurring with only a few degrees of freedom, for instance, with two coupled laser ring resonators[18,45] (Supplementary Information section XII). In the latter case, the state of the system switches between clockwise and anticlockwise under the effect of noise[45], destroying the chiral phase. This process also occurs in our systems for small N: it is captured by adding in equation (1) a hydrodynamic noise (Supplementary Information section X and Extended Data Fig. 2a). The average time τ between chirality flips follows an Arrhenius law, $\tau = \tau_0 \exp(\Delta/\sigma^2)$, where Δ is the height of the barrier between clockwise and anticlockwise states, σ is the standard deviation of the hydrodynamic noise, and τ_0 is a microscopic constant. For large N, the central limit theorem suggests that $\sigma^2 \sim 1/N$ (where $\sim$ indicates asymptotic behaviour; consistent with numerics in Supplementary Information sections VIII–X and Extended Data Fig. 2b) and $\tau \sim \exp(N)$. The chiral phase is salvaged by many-body effects. In optics, this scenario could be realized in non-reciprocal photonic networks of many coupled lasers[18,33,46–48].

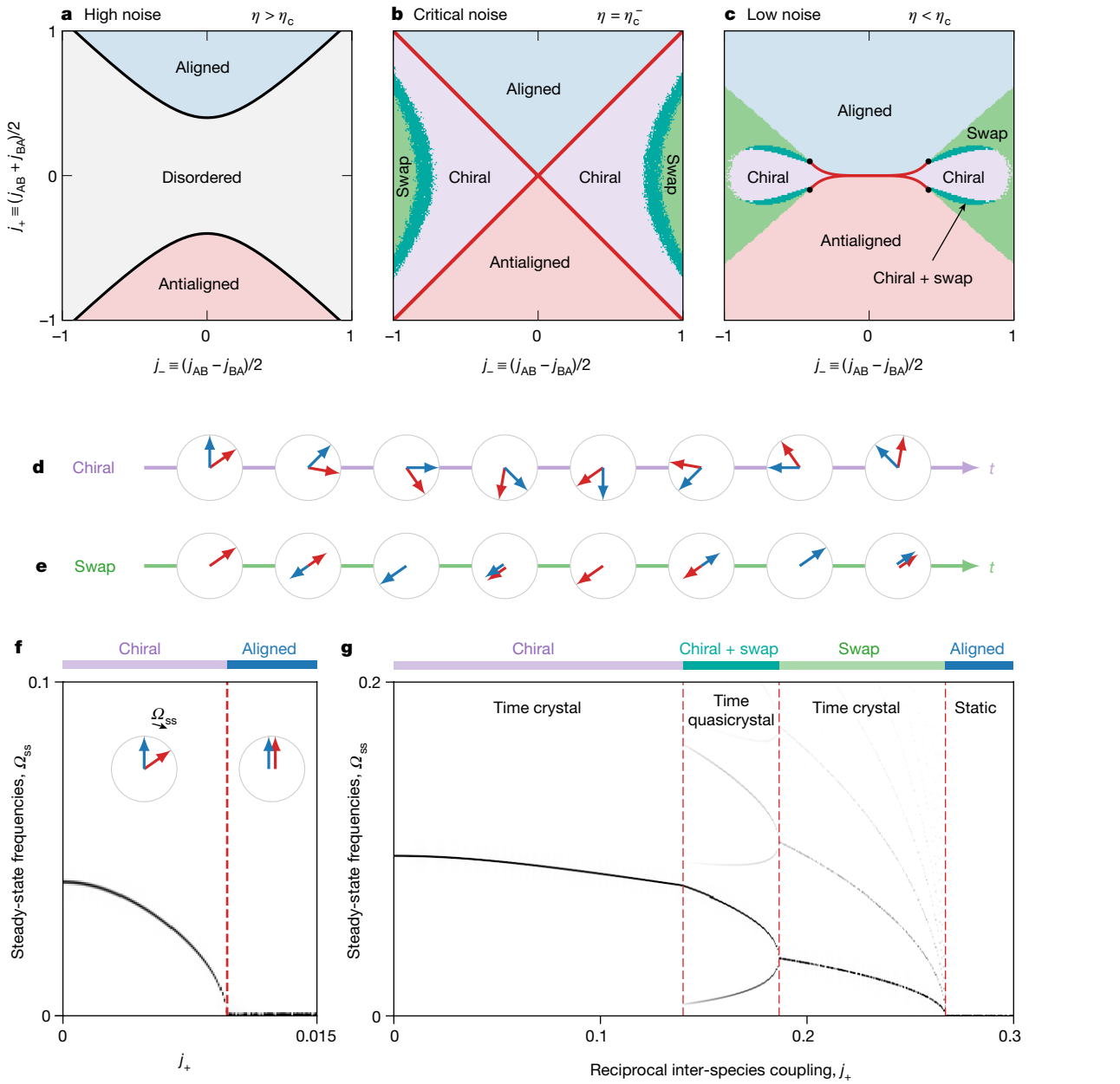

Fig. 2 | Phase diagrams and active time (quasi)crystals. a–**c**, Phase diagrams of the non-reciprocal flocking model Supplementary Information equation S83 for different noise strengths η. The parameters j_{ab} (entering α_{ab} and β_{abcd} in equation (1)) are coarse-grained versions of the microscopic couplings J_{ab}. The red (respectively, black) lines are analytically-determined transition lines from the (anti)aligned phase to the chiral (respectively, disordered) phase. Red lines are lines of exceptional points. The analytical prediction is in excellent agreement with the numerical phase diagram up to tetracritical points (black dots in **c**) where new phases emerge (Supplementary Information sections V–VI). **d**, Schematic representation of one period of the chiral phase: $\mathbf{v}_A$ and $\mathbf{v}_B$ rotate in block at a constant angular velocity Ω_{ss} (Supplementary Video 2). **e**, Schematic representation of one period of the swap phase: $\mathbf{v}_A$ and $\mathbf{v}_B$ oscillate along a fixed direction (Supplementary Video 2). **f**, **g**, Plot of the frequencies present in the steady state as a function of j_+, for $j_- = -0.25$ (**f**) and $j_- = -0.6$ (**g**). In the chiral phase, a single frequency is present (at each point), corresponding to the solid-body rotation. In the swap phase, a single frequency accompanied by harmonics are present. By contrast, in the mixed chiral/swap phase, two independent frequencies are present (with their harmonics), leading to a quasiperiodic phase. The aligned phase is static ($\Omega_{ss} = 0$). Similar behaviours occur around the antialigned phase. In **f**, a direct transition between aligned and chiral phases is observed. The phase diagrams are determined by solving Supplementary Information equation S83 numerically from random initial conditions, with $\rho_A = \rho_B = 1, j_{AA} = j_{BB} = 1$, and $\eta/\eta_c = 1.5$ (**a**), $\eta/\eta_c = 0.99$ (**b**), $\eta/\eta_c = 0.5$ (**c**). Parameters in **f**, **g** are the same as in **c**. All units are arbitrary.

The aligned-to-chiral transitions cannot be described by a free energy. This is in contrast with the familiar paramagnet-to-ferromagnet transition, or even mean-field descriptions of iconic non-equilibrium phase transitions such as directed percolation or (reciprocal) flocking (Supplementary Information section II). However, we can still identify the phases of the many-body system from the steady states of the corresponding dynamical system (such as equation (1)). Phase transitions occur when the steady state $\mathbf{V}_{ss}$ becomes unstable, that is, when perturbations around it are no longer damped. We therefore linearize equation (1), by separating the order parameters $\mathbf{V} \equiv (\mathbf{v}_A, \mathbf{v}_B, \ldots)$ into the steady state $\mathbf{V}_{ss}$ and the fluctuations $\delta\mathbf{V}$, leading to

$$\partial_t \delta\mathbf{V} = L\delta\mathbf{V}. \quad (5)$$

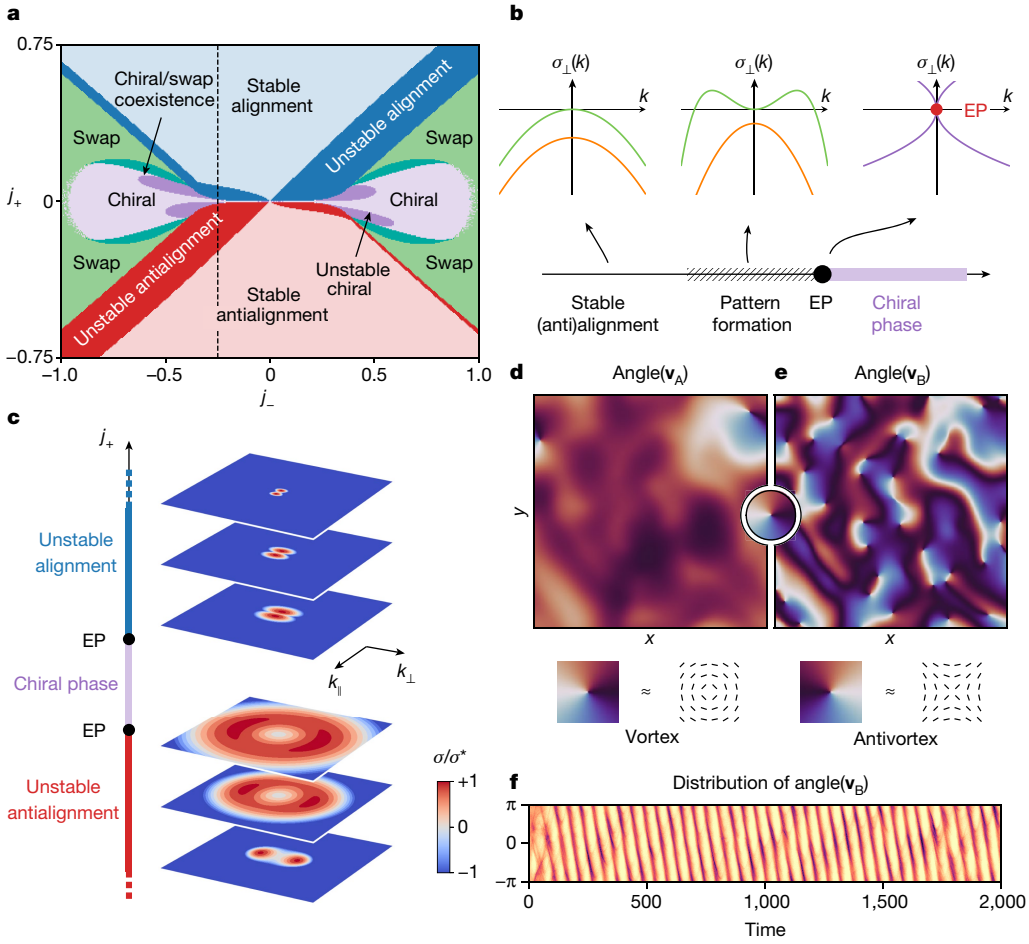

Fig. 3 | Exceptional-point-enforced pattern formation and topological defects. Convective terms and exceptional points (EPs) give rise to pattern formation near the transition lines. **a**, Numerical phase diagram including the linear stability analysis of the (anti)aligned and chiral phases in the non-reciprocal Toner–Tu model (the stability of the swap and chiral+swap phases is not analysed). Units are arbitrary. **b**, The coalescence of the Goldstone mode with a damped mode leads to instabilities at finite momentum. The growth rate of transverse perturbations $\sigma_\perp(k)$ becomes positive, and has a maximum σ^* at a finite wavevector k^*. **c**, Normalized growth rate $\sigma(k)/\sigma^*$ as a function of wavevector, for different values of j_+ at fixed j_+ (along the dashed line in **a**). **d**–**f**, Fully nonlinear simulation of the pattern formation in the unstable aligned regime. In **d**, **e**, we show snapshots of the angle of the order parameters $\mathbf{v}_A$ and $\mathbf{v}_B$ with a fixed direction (Supplementary Video 4). Numerous topological defects (vortices and antivortices) are present. In **f**, we show the time evolution (arbitrary units) of the histogram of the angle between $\mathbf{v}_A$ and a fixed direction ($\mathbf{v}_B$ has identical features). Parameters are the same as in Fig. 2 with $\eta/\eta_c = 0.5$. We set $v_A^0 = 0.06$ and $v_B^0 = 0.01$. Simulations in **d**–**f** are performed on a $2L \times 2L$ box with periodic boundary conditions, and $L = 0.32$, $j_+ = 0.1, j_- = 0.2$ (see Methods).

Non-reciprocity implies that the linear operator L can be non-Hermitian. For a conservative system, we would have $L_{ab} = -\partial_{\mathbf{v}_b}\partial_{\mathbf{v}_a}F = L_{ba}$. This implies that L is Hermitian, that is, $L_{ab} = L_{ba}$, as it is real-valued. A non-reciprocal system cannot be derived from an energy F, hence L is generally non-Hermitian, that is, $L_{ab} \neq L_{ba}$.

As a consequence, the eigenvectors of L need not be orthogonal. Its eigenvalues $s_i = \sigma_i + i\omega_i$ can be decomposed into growth rates σ_i and frequencies ω_i. Here, one eigenvalue always vanishes because it corresponds to a global rotation of the $\mathbf{v}_a$ (the Goldstone mode of broken rotation invariance), green line in Fig. 1h. In the static (anti)aligned phases, the other modes are always damped ($\sigma_i < 0$). The aligned–chiral transitions occur when the damped mode with σ_i closest to zero (orange line in Fig. 1h) coalesces with the Goldstone mode (green line) at red points. This mode coalescence is known as an exceptional point[21]. In addition to having the same (vanishing) eigenvalues, the two eigenmodes become parallel at the exceptional point. In a many-body system, the mode coalescence at an exceptional point defines a class of phase transitions that we dub exceptional transitions. Because of the non-orthogonality of the eigenmodes (Methods), these transitions are accompanied by enhanced fluctuations and distinctive critical phenomena[31,49–52].

The order parameter can be pictured as a ball constantly kicked by noise at the bottom of a sombrero potential. In a non-reciprocal system, there are transverse non-conservative forces in addition to the potential-energy landscape (Extended Data Fig. 3). When you kick the ball uphill (direction 1), it also moves perpendicular to the uphill direction along the bottom of the potential (direction 2), but not vice versa. At the exceptional point, the ball moves only along the bottom of the potential irrespective of how it is kicked: this is a signature of mode coalescence. It may be understood from the Jordan normal form $\mathbb{L}$ of an exceptional point,

$$\mathbb{L} = \begin{pmatrix} 0 & 0 \\ 1 & 0 \end{pmatrix}, \tag{6}$$

which describes a one-way coupling between the two directions: 1 influences 2 ($\mathbb{L}_{21} \neq 0$), whereas 2 has no influence on 1 ($\mathbb{L}_{12} = 0$). Non-reciprocity is inherent to exceptional points, irrespective of whether they originate from asymmetric microscopic interactions or gain/loss. Classical and quantum systems with gain and loss can indeed be mapped onto non-reciprocal ones: a non-Hermitian Hamiltonian H

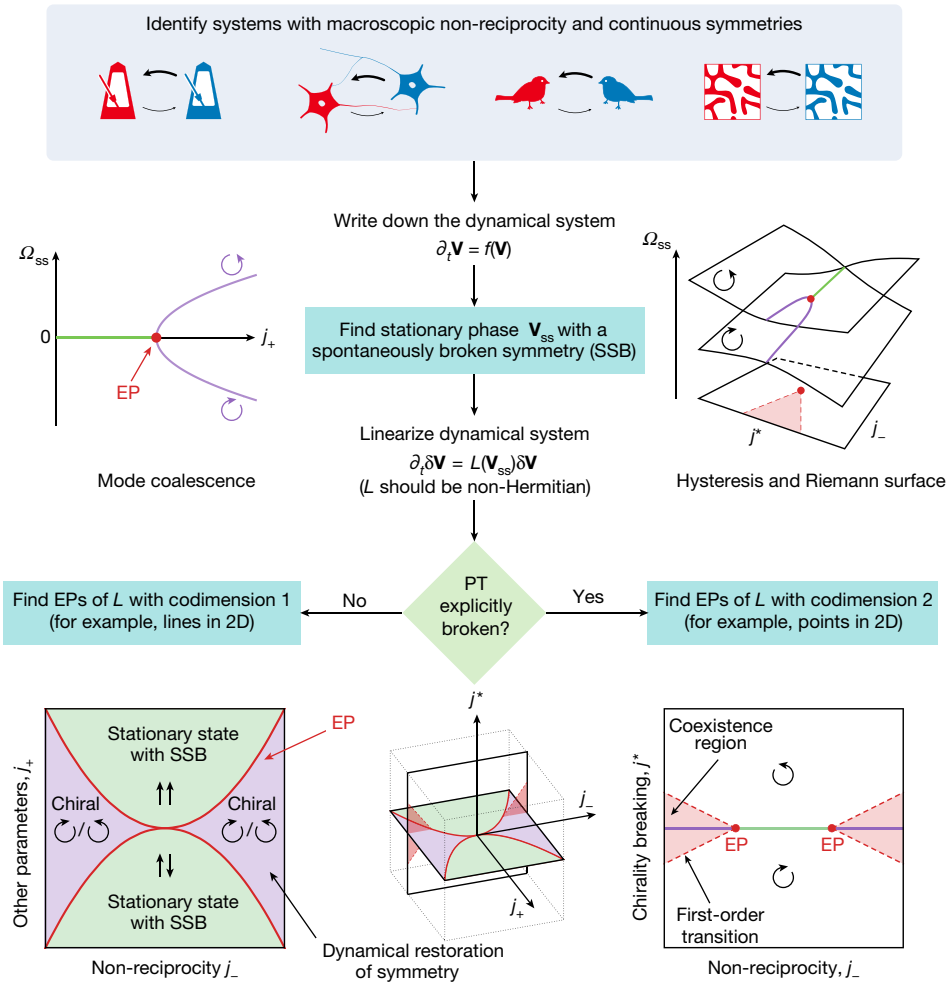

Fig. 4 | A visual procedure to identify and analyse exceptional transitions. First identify a system with (i) non-reciprocal interactions and (ii) a continuous symmetry. Write down the dynamical system for the order parameter(s) $\mathbf{V}$. Find a time-independent steady state $\mathbf{V}_{ss}$ with spontaneously broken continuous symmetry (SSB, green regions). Linearize around the time-independent steady state. The linear operator (Jacobian matrix) $L(\mathbf{V})$ has a vanishing eigenvalue (Goldstone mode). Exceptional points (EP; red points and continuous red lines) of $L(\mathbf{V})$ with zero eigenvalue mark the transition. We distinguish (I) parameters j that do not explicitly break parity and (II) parameters j^* that do. We further split the parameters j into (1) parameters j_- encoding the non-reciprocity and (2) other parameters j_+. When $j^* = 0$ (left panel), the exceptional points have codimension 1 (lines in a two-dimensional parameter space). At the exceptional transition, the Goldstone mode collides with a damped mode. This leads to a spontaneous dynamical restoration of symmetry (at the price of losing time-translation invariance). In the chiral phase (purple), the space of equivalent steady states (corresponding to the broken symmetry) is travelled in a direction chosen at random (clockwise or anticlockwise). When $j^* \neq 0$, this mechanism competes with an explicit rotation of the order parameter set by j^*. This leads to extended regions (light red) starting at the exceptional point (red point, now of codimension 2) in which the (anti)clockwise states coexist, marked by first-order transitions and hysteresis: the complex frequencies form a Riemann surface (Extended Data Fig. 5). Both cases are organized in a three-dimensional phase diagram (bottom, middle panel).

describing antisymmetric couplings is unitarily equivalent to a Hamiltonian with gain and loss as

$$H = \begin{pmatrix} 0 & 1 \\ -1 & 0 \end{pmatrix} \quad \Longleftrightarrow \quad UHU^{-1} = \begin{pmatrix} \mathrm{i} & 0 \\ 0 & -\mathrm{i} \end{pmatrix}, \tag{7}$$

in which U describes the change of basis. At an exceptional point, the non-reciprocal representation cannot be avoided as the matrix is not diagonalizable (like $\mathbb{L}$ in equation (6); see Supplementary Information section I).

Exceptional phase transitions in non-reciprocal matter (including many-body systems with gain and loss) can be viewed as dynamical restorations of a spontaneously broken continuous symmetry: the Goldstone mode is actuated by noise, and after the transition the system runs along the manifold of degenerate ground states. From the point of view of non-Hermitian quantum mechanics, these transitions are manifestations of spontaneous PT-symmetry breaking (Methods). From the point of view of dynamical systems, they are instances of Bogdanov–Takens bifurcations[23], with the peculiarity that one of the modes involved is a Goldstone mode (Methods).

As a concrete example, consider the hydrodynamics of non-reciprocal flocking (Supplementary Information equation S83). (Synchronization and pattern formation are treated in Methods.) Figure 2a–c shows the phase diagrams based on Supplementary Information equation S83 as a function of the rescaled (non-)reciprocal interspecies interactions $j_\pm = (j_{AB} \pm j_{BA})/2$ (Supplementary Information sections V–VI). There are disordered (grey), aligned (blue), antialigned (red) and chiral phases (purple; see also Fig. 2d). In Supplementary Information section VII, we prove that these phases are linearly stable against velocity fluctuations over large ranges of parameters. The phase boundary between chiral and (anti)aligned phases is marked by exceptional points (red lines in Fig. 2b, c).

Besides the chiral phase, we have identified a 'swap phase' (green region in Fig. 2b, c), where $\mathbf{v}_A$ and $\mathbf{v}_B$ oscillate along a fixed direction. In

contrast with the chiral phase, where a continuous symmetry is restored on average, the swap phase restores a discrete symmetry through the loss of time-translation invariance. We also predict and observe a mixed chiral+swap phase, where swap and chiral motions occur simultaneously (dark green region). These phases are illustrated in Fig. 2d, e and Supplementary Video 2: they all break time-translation invariance in a way reminiscent of time (quasi)crystals[53,54], Fig. 2f, g. The existence of all the phases in non-reciprocal flocking follows from symmetry principles[22]. Hence, they transcend specific models. We also observe them in non-reciprocal synchronization and pattern formation (Extended Data Figs. 4, 6).

In the presence of a steady-state flow $\mathbf{v}_{ss}$, non-reciprocal transitions exhibit pattern-forming instabilities around the mean-field critical lines (bright red and blue regions in Fig. 3a). This can be modelled by

$$\partial_t \delta\mathbf{V} = [L_{EP} + M(\mathbf{v}_{ss}\cdot\nabla) + D\nabla^2]\delta\mathbf{V}. \quad (8)$$

Equation (8) is a minimal extension of equation (5) valid near the transition. The singular matrix L_{EP} accounts for the exceptional point, and $M(\mathbf{v}_{ss}\cdot\nabla)$ and $D\nabla^2$ model convection (mixing species through M) and diffusion, respectively. Because the eigenvalues of a perturbed exceptional point typically behave as the square root of the perturbation[21], the complex growth rate of the momentum space behaves as $s_{\pm}(k) \approx \pm \mathrm{i}\sqrt{\mathrm{i}v_{ss}\,k}$ at small wavevector k (where $v_{ss} = |\mathbf{v}_{ss}|$) and as $-Dk^2$ at large k. This leads to a maximum in the growth rate, that is, a linear instability at finite momentum (Fig. 3b, c). Figure 3d–f and Supplementary Videos 4, 5 provide glimpses into the nonlinear regime of pattern formation. Vortex pairs continuously unbind and annihilate with different densities in $\mathbf{v}_A$ and $\mathbf{v}_B$ set by the different self-propulsion speeds (Fig. 3d, e). The system does not coarsen, and its nearly periodic average evolution (Fig. 3f) is a precursor of the chiral phase.

Although parity is spontaneously broken in the chiral phase, it is explicitly broken in, for example: (i) the Kuramoto model with nonvanishing natural frequencies; (ii) the Vicsek model with external torques; and (iii) the Swift–Hohenberg model with broken up–down ($u \to -u$) symmetry. All these systems still fit in the framework of equation (1), provided that the matrices $\mathbb{A}^{\mu\nu}_{ab}$ and $\mathbb{B}^{\mu\nu}_{abcd}$ acting on $\mathbf{v}^{\nu}_{a}(t,x)$ are appropriately chosen (μ and ν denote vector components). Rotational symmetry determines the form of these matrices: $\mathbb{A}^{\mu\nu}_{ab} = \alpha_{ab}\delta^{\mu\nu} + \alpha^*_{ab}\epsilon^{\mu\nu}$ and $\mathbb{B}^{\mu\nu}_{abcd} = \beta_{abcd}\delta^{\mu\nu} + \beta^*_{abcd}\epsilon^{\mu\nu}$, where α, β, α^* and β^* are arbitrary coefficients. Here, $\delta^{\mu\nu}$ is the identity and $\epsilon^{\mu\nu}$ is an antisymmetric matrix that rotates vectors by 90°. We classify: (I) parity symmetric systems in which α^* and β^* vanish; and (II) systems in which parity is explicitly broken, in which α^* and β^* can be non-zero. Classes I and II encompass systems invariant under general O(2) and proper SO(2) rotations, respectively.

In the language of non-Hermitian quantum mechanics[18,24,25], class I exhibits (generalized) PT symmetry, which may be spontaneously broken in the chiral phase; the transition has codimension one (for example, Fig. 2). In class II, PT symmetry is explicitly broken: (anti) aligned phases rotate and the exceptional points have codimension two (Extended Data Fig. 5 and Fig. 4). In Methods, we analyse the non-reciprocal Kuramoto model (2) with $\omega_m \neq 0$. Non-reciprocity and explicit PT-symmetry breaking lead to hysteresis and discontinuous transitions between regions where (i) states with opposite chiralities coexist and (ii) only one state exists (Extended Data Fig. 5). These results reveal a remarkable similarity between non-reciprocal synchronization and driven quantum condensates[30,31], both of which are encompassed by equation (1) and span classes I and II.

Figure 4 summarizes a visual procedure to extend our approach to other systems. The key ingredients are (i) non-reciprocity manifested in asymmetric macroscopic couplings and (ii) a spontaneously broken continuous symmetry. Non-reciprocal transitions can occur for any continuous group. For example, the spherical symmetry O(3) relevant to three-dimensional flocks is discussed in Supplementary Information section XI. Our analysis was illustrated with vector order parameters whose evolution is not the expression of a conservation law. This paradigmatic case is known as model A in the Hohenberg–Halperin classification of dynamical critical phenomena[32]. The same approach applies also to other order parameters and classes—see ref. [19] for a non-reciprocal active elasticity that conserves linear momentum and refs. [55,56] for non-reciprocal models of phase separation that conserve mass (both illustrate model B in the language of ref. [32]).

Our work lays the foundation for a general theory of critical phenomena in non-reciprocal matter, from driven quantum condensates to biological and artificial neural networks. These systems are marked by the interplay between non-reciprocal enhancement of fluctuations and rigidity bestowed by many-body effects. Our field-theoretical approach captures these effects and builds new bridges between many-body physics and bifurcation theory.

Online content

Any methods, additional references, Nature Research reporting summaries, source data, extended data, supplementary information, acknowledgements, peer review information; details of author contributions and competing interests; and statements of data and code availability are available at https://doi.org/10.1038/s41586-021-03375-9.

1. Shankar, S., Souslov, A., Bowick, M. J., Marchetti, M. C. & Vitelli, V. Topological active matter. Preprint at https://arxiv.org/abs/2010.00364 (2020).
2. Uchida, N. & Golestanian, R. Synchronization and collective dynamics in a carpet of microfluidic rotors. *Phys. Rev. Lett.* **104**, 178103 (2010).
3. Saha, S., Ramaswamy, S. & Golestanian, R. Pairing, waltzing and scattering of chemotactic active colloids. *New J. Phys.* **21**, 063006 (2019).
4. Nagy, M., Ákos, Z., Biro, D. & Vicsek, T. Hierarchical group dynamics in pigeon flocks. *Nature* **464**, 890–893 (2010).
5. Yllanes, D., Leoni, M. & Marchetti, M. C. How many dissenters does it take to disorder a flock? *New J. Phys.* **19**, 103026 (2017).
6. Lavergne, F. A., Wendehenne, H., Bäuerle, T. & Bechinger, C. Group formation and cohesion of active particles with visual perception–dependent motility. *Science* **364**, 70–74 (2019).
7. van Zuiden, B. C., Paulose, J., Irvine, W. T. M., Bartolo, D. & Vitelli, V. Spatiotemporal order and emergent edge currents in active spinner materials. *Proc. Natl Acad. Sci. USA* **113**, 12919 (2016).
8. Ivlev, A. V. et al. Statistical mechanics where Newton's third law is broken. *Phys. Rev. X* **5**, 011035 (2015).
9. Lahiri, R. & Ramaswamy, S. Are steadily moving crystals unstable? *Phys. Rev. Lett.* **79**, 1150–1153 (1997).
10. Montbrió, E. & Pazó, D. Kuramoto model for excitation-inhibition-based oscillations. *Phys. Rev. Lett.* **120**, 244101 (2018).
11. Sompolinsky, H. & Kanter, I. Temporal association in asymmetric neural networks. *Phys. Rev. Lett.* **57**, 2861–2864 (1986).
12. Hong, H. & Strogatz, S. H. Kuramoto model of coupled oscillators with positive and negative coupling parameters: an example of conformist and contrarian oscillators. *Phys. Rev. Lett.* **106**, 054102 (2011).
13. Malomed, B. & Tribelsky, M. Bifurcations in distributed kinetic systems with aperiodic instability. *Physica D* **14**, 67–87 (1984).
14. Coullet, P., Goldstein, R. E. & Gunaratne, G. H. Parity-breaking transitions of modulated patterns in hydrodynamic systems. *Phys. Rev. Lett.* **63**, 1954–1957 (1989).
15. Pan, L. & de Bruyn, J. R. Spatially uniform traveling cellular patterns at a driven interface. *Phys. Rev. E* **49**, 483–493 (1994).
16. Fleury, R., Sounas, D. L., Sieck, C. F., Haberman, M. R. & Alù, A. Sound isolation and giant linear nonreciprocity in a compact acoustic circulator. *Science* **343**, 516–519 (2014).
17. Brandenbourger, M., Locsin, X., Lerner, E. & Coulais, C. Non-reciprocal robotic metamaterials. *Nat. Commun.* **10**, 4608 (2019).
18. Miri, M.-A. & Alù, A. Exceptional points in optics and photonics. *Science* **363**, eaar7709 (2019).
19. Scheibner, C. et al. Odd elasticity. *Nat. Phys.* **16**, 475–480 (2020).
20. Helbig, T. et al. Generalized bulk–boundary correspondence in non-Hermitian topolectrical circuits. *Nat. Phys.* **16**, 747–750 (2020).
21. Kato, T. *Perturbation Theory for Linear Operators* 2nd edn (Springer, 1984).
22. Golubitsky, M. & Stewart, I. *The Symmetry Perspective* (Birkhäuser, 2002).
23. Kuznetsov, Y. A. *Elements of Applied Bifurcation Theory* (Springer, 2004).
24. Hatano, N. & Nelson, D. R. Localization transitions in non-Hermitian quantum mechanics. *Phys. Rev. Lett.* **77**, 570–573 (1996).
25. Bender, C. M. & Boettcher, S. Real spectra in non-Hermitian Hamiltonians having PT symmetry. *Phys. Rev. Lett.* **80**, 5243–5246 (1998).
26. Bricard, A., Caussin, J.-B., Desreumaux, N., Dauchot, O. & Bartolo, D. Emergence of macroscopic directed motion in populations of motile colloids. *Nature* **503**, 95–98 (2013).
27. Palacci, J., Sacanna, S., Steinberg, A. P., Pine, D. J. & Chaikin, P. M. Living crystals of light-activated colloidal surfers. *Science* **339**, 936–940 (2013).

28. Sieberer, L. M., Huber, S. D., Altman, E. & Diehl, S. Dynamical critical phenomena in driven-dissipative systems. *Phys. Rev. Lett*. **110**, 195301 (2013).
29. Metelmann, A. & Clerk, A. A. Nonreciprocal photon transmission and amplification via reservoir engineering. *Phys. Rev. X* **5**, 021025 (2015).
30. Hanai, R., Edelman, A., Ohashi, Y. & Littlewood, P. B. Non-Hermitian phase transition from a polariton Bose–Einstein condensate to a photon laser. *Phys. Rev. Lett*. **122**, 185301 (2019).
31. Hanai, R. & Littlewood, P. B. Critical fluctuations at a many-body exceptional point. *Phys. Rev. Res*. **2**, 033018 (2020).
32. Hohenberg, P. C. & Halperin, B. I. Theory of dynamic critical phenomena. *Rev. Mod. Phys*. **49**, 435–479 (1977).
33. Acebrón, J. A., Bonilla, L. L., Vicente, C. J. P., Ritort, F. & Spigler, R. The Kuramoto model: a simple paradigm for synchronization phenomena. *Rev. Mod. Phys*. **77**, 137–185 (2005).
34. Vicsek, T., Czirók, A., Ben-Jacob, E., Cohen, I. & Shochet, O. Novel type of phase transition in a system of self-driven particles. *Phys. Rev. Lett*. **75**, 1226–1229 (1995).
35. Toner, J. & Tu, Y. Long-range order in a two-dimensional dynamical *XY* model: how birds fly together. *Phys. Rev. Lett*. **75**, 4326–4329 (1995).
36. Sakaguchi, H. & Kuramoto, Y. A soluble active rotater model showing phase transitions via mutual entertainment. *Prog. Theor. Phys*. **76**, 576–581 (1986).
37. Daido, H. Quasientrainment and slow relaxation in a population of oscillators with random and frustrated interactions. *Phys. Rev. Lett*. **68**, 1073–1076 (1992).
38. Das, J., Rao, M. & Ramaswamy, S. Driven Heisenberg magnets: nonequilibrium criticality, spatiotemporal chaos and control. *Europhys. Lett*. **60**, 418–424 (2002).
39. Bonilla, L. L. & Trenado, C. Contrarian compulsions produce exotic time-dependent flocking of active particles. *Phys. Rev. E* **99**, 012612 (2019).
40. Cross, M. C. & Hohenberg, P. C. Pattern formation outside of equilibrium. *Rev. Mod. Phys*. **65**, 851–1112 (1993).
41. Rabaud, M., Michalland, S. & Couder, Y. Dynamical regimes of directional viscous fingering: spatiotemporal chaos and wave propagation. *Phys. Rev. Lett*. **64**, 184–187 (1990).
42. Oswald, P., Bechhoefer, J. & Libchaber, A. Instabilities of a moving nematic–isotropic interface. *Phys. Rev. Lett*. **58**, 2318–2321 (1987).
43. Faivre, G., de Cheveigne, S., Guthmann, C. & Kurowski, P. Solitary tilt waves in thin lamellar eutectics. *Europhys. Lett*. **9**, 779–784 (1989).
44. Brunet, P., Flesselles, J.-M. & Limat, L. Parity breaking in a one-dimensional pattern: a quantitative study with controlled wavelength. *Europhys. Lett*. **56**, 221–227 (2001).
45. Hassan, A. U., Hodaei, H., Miri, M.-A., Khajavikhan, M. & Christodoulides, D. N. Nonlinear reversal of the PT-symmetric phase transition in a system of coupled semiconductor microring resonators. *Phys. Rev. A* **92**, 063807 (2015).
46. Nixon, M., Ronen, E., Friesem, A. A. & Davidson, N. Observing geometric frustration with thousands of coupled lasers. *Phys. Rev. Lett*. **110**, 184102 (2013).
47. Parto, M., Hayenga, W., Marandi, A., Christodoulides, D. N. & Khajavikhan, M. Realizing spin Hamiltonians in nanoscale active photonic lattices. *Nat. Mater*. **19**, 725–731 (2020).
48. Ramos, A., Fernández-Alcázar, L., Kottos, T. & Shapiro, B. Optical phase transitions in photonic networks: a spin-system formulation. *Phys. Rev. X* **10**, 031024 (2020).
49. Ashida, Y., Furukawa, S. & Ueda, M. Parity-time-symmetric quantum critical phenomena. *Nat. Commun*. **8**, 15791 (2017).
50. Strack, P. & Vitelli, V. Soft quantum vibrations of a PT-symmetric nonlinear ion chain. *Phys. Rev. A* **88**, 053408 (2013).
51. Biancalani, T., Jafarpour, F. & Goldenfeld, N. Giant amplification of noise in fluctuation-induced pattern formation. *Phys. Rev. Lett*. **118**, 018101 (2017).
52. Trefethen, L. N., Trefethen, A. E., Reddy, S. C. & Driscoll, T. A. Hydrodynamic stability without eigenvalues. *Science* **261**, 578–584 (1993).
53. Winfree, A. T. *The Geometry of Biological Time* (Springer, 2001).
54. Khemani, V., Moessner, R. & Sondhi, S. L. A brief history of time crystals. Preprint at https://arxiv.org/abs/1910.10745 (2019).
55. You, Z., Baskaran, A. & Marchetti, M. C. Nonreciprocity as a generic route to traveling states. Preprint at https://arxiv.org/abs/2005.07684 (2020).
56. Saha, S., Agudo-Canalejo, J. & Golestanian, R. Scalar active mixtures: the nonreciprocal Cahn–Hilliard model. Preprint at https://arxiv.org/abs/2005.07101 (2020).

Methods

Phase transitions and bifurcations of dynamical systems

Equilibrium phase transitions are usually described in terms of a free energy. The minimum of the free energy corresponds to the current phase, and a phase transition occurs when it ceases to be a global minimum, or a minimum at all. Although this landscape picture is static, it relies on an underlying dynamics that shepherds the system into the global minimum in a way or another[32,40,57–59]. The simplest dynamics is relaxational. In this case, the dynamical system that describes the time evolution of the order parameter ϕ near its equilibrium value reads[32,40,57,60,61]

$$\frac{\partial \phi}{\partial t} = -\frac{\delta F}{\delta \phi} \tag{9}$$

for a system described by the Ginzburg–Landau free energy $F[\phi]$ (or a Ginzburg–Landau–Wilson Hamiltonian obtained from microscopics)[61,62]. Phase transitions can be seen as bifurcations of this dynamical system[63–65]. (See also refs. [40,61,66,67] on non-equilibrium pattern formation. We refer to ref. [40], section III.A.5 for a discussion on the difference between bifurcations and thermodynamic phase transitions; here, we will liberally use the term 'phase transition' to describe both situations.)

Instead of starting with a free energy, one can take a general (possibly spatially extended) dynamical system

$$\partial_t \phi = f(\phi) \tag{10}$$

as a starting point, generalizing equation (9). (Here, f can be a functional of the field ϕ.) This approach extends the Landau theory of phase transitions to non-equilibrium systems not described by a free energy. The dynamical system in equation (10) can be constructed from symmetry arguments, in the same way as a Landau–Ginzburg free energy, using the methods of equivariant dynamical systems[22,68–71].

We emphasize that the exceptional transition defined in the main text cannot be described by a free energy even at the mean-field level, putting it apart from equlibrium phase transitions, but also from standard non-equilibrium phase transitions[72–76] such as the flocking transition[35,77] or the directed percolation transition[73]. These can be described by a free-energy at the mean field level (their non-equilibrium character is contained elsewhere, for example, in the noise).

More generally, there are bifurcations possible within the relaxational dynamics of equation (10) that cannot occur when the form of the dynamical system is restricted to equation (9). In the context of a many-body system, these correspond to phase transitions that are forbidden at equilibrium (within a relaxational dynamics). The exceptional transitions described in the main text are an example of this phenomenon.

Non-reciprocity out of equilibrium

In this section, we discuss the relations between non-reciprocity, the non-Hermitian (non-normal) character of the Jacobian of a dynamical system, which allows it to exhibit an exceptional point, and the non-equilibrium character of the system.

A dynamical system $\partial_t X = f(X)$ is said to be conservative when it derives from some potential F (for example, a free energy), such that $f_a(X) = -\partial_{X_a} F$. (Here, we assume that X is real.) The Jacobian of the dynamical system is defined as the real matrix $L_{ab} = \partial_{X_b} f_a$. When the dynamical system is conservative, $L_{ab} = -\partial_{X_b}\partial_{X_a} F = L_{ba}$ is symmetric, and hence it is a normal operator. When the dynamical system is not conservative, it is possible to have $L_{ab} \neq L_{ba}$, that is, L is not symmetric. This is our operational definition of non-reciprocity. In the language of quantum mechanics, we would say that the operator is non-Hermitian (because it could be complex-valued). The key point is that L is not a normal operator (a matrix N is normal when it is unitarily diagonalizable; equivalently, $N^\dagger N = N N^\dagger$, where † indicates the conjugate transpose; see ref. [78]). Deviations from normality allow the eigenvectors of L not to be orthogonal, leading to a variety of physical consequences related to transient growths and an enhanced sensitivity to fluctuations, in hydrodynamics[52,79–87], (general and neural) networks[88–94], ecological systems[51,95–99], photonics[18,100,101], and quantum systems[24,25,31,49,102–105]. In particular, the presence of exceptional points requires a non-normal operator.

Note that the notion of normality depends on the choice of the scalar product and the associated norm (this is also true for symmetry and Hermiticity). Equivalently, these notions are not invariant under a generic invertible change of basis (see Supplementary Information section I for an example), although a certain scalar product might be selected by physical considerations. By contrast, the presence of an exceptional point and the notions of spontaneously/explicitly/not-broken generalized PT symmetry (see Supplementary Information section III for a discussion of generalized PT symmetry in this context, including refs. [25,106–115]) are independent of the choice of the basis. Indeed, exceptional points represent an ultimate, unavoidable form of non-reciprocity (and non-normality). As equation (6) highlights, they describe a one-way coupling between the two degrees of freedom in which the Jordan normal-form matrix is written.

Non-reciprocity is also related to the breaking of detailed balance (that is, microscopic reversibility). The notion of detailed balance deals with stochastic processes, hence we have to consider a stochastic dynamical system $\partial_t X = f(X) + \eta(t)$, where $\eta(t)$ is a noise. This can either represent a microscopic system or a fluctuating hydrodynamic equation. Assuming that the noise is scalar, detailed balance implies (that is, requires) that $\partial_{X_a} f_b = \partial_{X_b} f_a$ (that is, $L_{ab} = L_{ba}$). (See Supplementary Information section IV and references therein, including refs. [116–120]. When the noise is not scalar, this equality is weighted by the corresponding diffusion constants.)

The concepts of 'non-conservative dynamical systems' and 'non-conserved order parameters' discussed in the main text are completely unrelated. (Their names are borrowed from conservative forces and conserved quantities.) Following the classification of ref. [32], we talk about a conserved order parameter ('model B' in ref. [32]) when its dynamics is the expression of a conservation law (for example, conservation of mass). When this is not the case, we say that the order parameter is not conserved ('model A' in ref. [32]). In parallel, a dynamical system is conservative when it derives from a potential, as discussed in the previous paragraph.

Let us now discuss connections between the notions discussed above and more general notions of non-reciprocity. Broadly, non-reciprocity occurs when A does not have the same effect on B as does B on A. This can often lead to a non-conservative dynamical system as defined above, but the connection is not systematic.

Newton's third law[121] states that the force f_{ij} that an object i exerts on an object j is exactly opposite to the force f_{ji} than j exerts on i (that is, $f_{ij} = -f_{ji}$). This symmetry between action and reaction can be violated when the interaction between the objects is mediated by an non-equilibrium environment. Such non-reciprocal interactions can arise in various contexts: particles in fluids[9,87,122–124], non-equilibrium plasma[8,125], chemically and biologically active matter[2,3,126,127], optical matter[128–130], networks of neurons[10,11,90,131–134], social groups[12,135,136], and so on. The symmetry between action and reaction has no particular reason to occur in complex systems in which the interactions summarize the decisions of agents/algorithms: it is explicitly violated in active matter[5,9,137–142], for example, for biological reasons such as a limited vision cone[6,143,144] or hierarchical relationships[4], as well as in systems with synthetic physical interactions[3,8,19,125,126,145] or programmable robotic interactions[17,146–149]. The non-equilibrium character of such non-conservative forces leads to diverse but crucial consequences on the behaviour of the corresponding systems[8,38,139,150–154].

In condensed matter, in particular in the context of topological insulators, non-symmetric tight-binding Hamiltonians $H \neq H^{\mathrm{T}}$ (where

T indicates the transpose) with non-symmetric hopping terms (leading to non-Hermitian Hamiltonians in momentum space) are called non-reciprocal; see refs. [20,24,96,155–161]. In an elastic network, the Hamiltonian is replaced by a dynamical matrix D such that the force F_i^μ on the particle i is $F_i^\mu = -D_{ij}^{\mu\nu}u_j^\nu$ (with u_j^ν the displacement of the particle j with respect to its equilibrium position). The overdamped dynamics of such a system is ruled by an equation of the form $\gamma\partial_t u_i^\mu = D_{ij}^{\mu\nu}u_j^\nu$. In this case, the symmetry of the dynamical matrix indeed corresponds to reciprocity as we have defined in the first paragraph, and is associated with a non-conservative dynamical system. Non-reciprocity ($D \neq D^T$) can occur through a violation of Newton's third law by which $D_{ij} \neq D_{ji}$ (see for example, ref. [17]), or through 'odd springs' with transverse responses by which $D^{\mu\nu} \neq D^{\nu\mu}$ (see ref. [19]). In both cases, some degree of activity is required (energy is not conserved), and the noisy overdamped dynamics again exhibits broken detailed balance.

At the level of responses, reciprocity is captured by various notions that share many similarities, such as Maxwell–Betti reciprocity in elasticity and acoustics[16,162,163], Lorentz reciprocity in optics[164–166]. Similar relations appear also in fluid dynamics and other fields[167]. For instance, the non-reciprocal elastic networks (with $D \neq D^T$) in refs. [17,19,149,168,169] violate Maxwell–Betti reciprocity. A similar notion exists in non-equilibrium thermodynamics: Onsager reciprocal relations are the statement that the matrix of response coefficients L relating thermodynamic fluxes J_i and forces $\mathcal{F}_k$ through $J_i = L_{ik}\mathcal{F}_k$ is symmetric (more precisely, the Onsager–Casimir relations state that $L_{ik}(B) = \epsilon_i\epsilon_k L_{ki}(-B)$ where $\epsilon_i = \pm 1$ depending on whether the quantity i is even/odd with respect to time reversal, and where B represents all external time-reversal breaking fields such as magnetic fields and rotations)[170,171]. This relation is also a consequence of microscopic reversibility. Depending on the system, L contains the diffusion coefficients, electric conductivities, viscosities, and so on. For example, Hall conductivity and odd viscosity[170,172–176] are instances of antisymmetric components that require broken detailed balance.

Exceptional transitions and Bogdanov–Takens bifurcations

In this section, we discuss our results from the point of view of bifurcation theory[22,23,68,69,71,177]. The exceptional transitions analysed in the main text are closely related to Bogdanov–Takens (BT) bifurcations[23,178–180]. A difference compared to usual BT bifurcations is that exceptional transitions are secondary bifurcations from a state with a spontaneously broken continuous symmetry. In both cases, the linearized dynamics (the Jacobian of the dynamical system) has a vanishing eigenvalue of algebraic multiplicity two $\lambda_1 = \lambda_2 = 0$ associated with a Jordan block of size two, that is, an exceptional point. In the case of exceptional transitions, the Goldstone theorem[181–187] guarantees that a so-called Nambu–Goldstone mode with vanishing frequency and growth rate at large wavelength always exists because of the spontaneously broken continuous symmetry, corresponding to a vanishing eigenvalue $\lambda_1 = 0$ in a time-independent state. (Note that the Goldstone theorem applies to dynamical systems, not only Hamiltonian systems; see refs. [185,188–190].) As a consequence, the codimension of exceptional transitions (the number of parameters typically required to get to the bifurcation) is one in class I (in the Supplementary Information, we show that this occurs generically when O(2) symmetry is preserved). This should be contrasted with the codimension two of standard BT bifurcations, which is here reduced by one because of the presence of the Goldstone mode. In class II, time-independent states do not form a submanifold of codimension zero, and the codimension of the bifurcation is increased again. Correspondingly, exceptional transitions occur along lines in the two-dimensional phase diagram Fig. 2b, c, but at points in Extended Data Fig. 5.

More precisely, the degeneracy $\lambda_1 = \lambda_2 = 0$ can occur in two ways (see refs. [191–194] and Extended Data Fig. 1 on the problem of the codimension of subspaces with equal eigenvalues): at an exceptional point where the eigenvectors become collinear, or at a diabolic/Dirac point (DP) where the eigenvectors stay linearly independent. DPs have a higher codimension than exceptional points (so they can essentially be ignored), and do not correspond to the BT bifurcation (see, for example, refs. [195,196] for the corresponding codimension-4 bifurcation). For real matrices, the codimension of exceptional points is one. Along with the condition that the degenerate eigenvalue must vanish, this gives a codimension two to BT bifurcations. The presence of the Goldstone mode fixes one eigenvalue λ_1 to zero, reducing the codimension by one (strictly speaking, to the codimension of exceptional points in the space of matrices with at least one zero eigenvalue, and this corresponds to a reduction by one).

We note that exceptional transitions are not BT bifurcations with O(2) symmetry in the sense of refs. [197,198], as the stable eigenvalues $0 < \lambda_3 \neq \lambda_4$ are generally different. This is because we consider the departure from an ordered state with spontaneous symmetry breaking (aligned phase), not from a fully symmetric state (disordered phase). (This could be analysed as a secondary bifurcation through mode interactions[22,68,69] or with the formalism of refs. [199,200].)

Hydrodynamic theory for non-reciprocal flocking

We have derived hydrodynamic equations for the densities $\rho_a(t, \mathbf{x})$ and polarizations $\mathbf{P}_a(t, \mathbf{x})$ (or equivalently the velocities $\mathbf{v}_a(t, \mathbf{x})$; in the main text, we denote the polarization fields by $\mathbf{v}_a(t, \mathbf{x})$ for simplicity) of an arbitrary number of populations from equations (2), (3). For a single population, the microscopic model reduces to the Vicsek model and the hydrodynamic theory to the Toner–Tu field theory, both of which describe flocking[26,27,34,35,201–203]. Our derivation, presented in Supplementary Information section V, follows the methods described in refs. [5,77,204–208]. More elaborate methods of coarse-graining exist[205,206,209,210], but current state-of-the-art procedures only provide a qualitative agreement with the microscopic starting point[208,211]. Hence, we use the the easiest method, along with several simplifying approximations (see Supplementary Information section V), to highlight the key features of a non-reciprocal multi-component fluid, without looking for a quantitative agreement (in the sense that the values of the coefficients might be inaccurate). The set of hydrodynamic equations obtained generalize the Toner–Tu equations[35,201] to any number of populations with non-reciprocal interactions, and are the basis of the analysis in the main text.

Our results for two populations also generalize the situation considered in ref. [5], which considers aligners A (standard Vicsek-like self-propelling particles) and dissenters B that do not align at all with anyone (neither A nor B), but with which the population A aligns. With our notations, this corresponds to $j_{AA}, j_{AB} > 0$ but $j_{BB} = j_{BA} = 0$.

The full hydrodynamic equations for two populations a = A, B are given in Supplementary Information equation S83 (Supplementary Information section V.C.2). For uniform fields, gradient terms can be removed and equation S83 reduces to

$$\partial_t \begin{pmatrix} \mathbf{P}_A \\ \mathbf{P}_B \end{pmatrix} = \begin{pmatrix} \gamma_A[\mathbf{P}_A, \mathbf{P}_B] & j_{AB}\rho_A \\ j_{BA}\rho_B & \gamma_B[\mathbf{P}_A, \mathbf{P}_B] \end{pmatrix} \begin{pmatrix} \mathbf{P}_A \\ \mathbf{P}_B \end{pmatrix}, \tag{11}$$

where

$$\gamma_A = j_{AA}\rho_A - \eta - \frac{1}{2\eta}\|j_{AA}\mathbf{P}_A + j_{AB}\mathbf{P}_B\|^2 \tag{12}$$

and similarly for B, and where $j_{ab} = \frac{R_0^2}{2}J_{ab}$. Here, R_0 is a characteristic length scale of the interaction. (The polarizations denoted by $\mathbf{P}_A$ and $\mathbf{P}_B$ here and in the Supplementary Information are called $\mathbf{v}_A$ and $\mathbf{v}_B$ in the main text.) This equation is used to construct the phase diagrams of Fig. 2; see Supplementary Information section VI. We find (a) a disordered regime where the order parameter vanishes, (b) a flocking regime where the order parameters are parallel, (c) an antiflocking regime where the order parameters are antiparellel (sharing some similarities with refs. [212–214]), (d) a periodic chiral regime where the

order parameter have circular trajectories (sharing similarities with chiral active matter[173–176,215–218]), (e) a periodic swap regime where the order parameter oscillate along a fixed direction, (f) a quasiperiodic chiral+swap regime in which the order parameter oscillates along a rotating direction. The full Supplementary Information equation S83 including gradient terms is then linearized above the uniform solution of equation (11) to obtain the stability diagram of Fig. 3 (see Supplementary Information section VII for details on the computations). We perform numerical simulation of the same Supplementary Information equation S83 using the open-source pseudospectral solver Dedalus[219] to analyse the pattern formation regime in Fig. 3d–f (see Supplementary Information section XV for details). In all cases, the densities ρ_a are assumed to be constant (this occurs, for instance, in the incompressible limit); when this is not the case, other instabilities can occur[26,220–223].

Non-reciprocal Kuramoto model

In this section, we provide details on the analysis of the non-reciprocal Kuramoto model[2,12,33,36,37,135,224–235]. Depending on whether the system is in class I or in class II (respectively, PT symmetric and non-PT symmetric), we find codimension-1 or codimension-2 exceptional points, respectively, around which the phase diagram is organized. In class I, the exceptional line (in a two-dimensional phase diagram) separates the static (aligned or antialigned) phases from a chiral phase where parity (equivalent here to PT symmetry) is spontaneously broken. (See Supplementary Information section III for a discussion of generalized PT symmetry in the equivariant dynamical systems considered here.) In class II, an exceptional point structures the phase diagram: the stable steady states are organized on a truncated version of the Riemann surface of the square root. This leads to discontinuous transitions marked by hysteresis between regions where two stable states coexist and regions where only one state exists, in a similar manner to driven-dissipative quantum fluids[30,31]. We first present analytic self-consistency arguments in which the existence of a static or harmonic steady state is assumed. We then resort to numerical simulations of a reduced dynamical system to confirm our analytic predictions and explore the full phase diagram, including non-harmonic time-dependent phases.

We start from equation (2), in which we consider globally coupled (all-to-all) oscillators and neglect the noise $\eta(t) \equiv 0$, as in the original Kuramoto model. The oscillators are separated into two communities (species) A and B and their phases follow

$$\partial_t \theta_m^a = \omega_m^a + \sum_b \sum_{n=1}^{N_b} J_{ab} \sin(\theta_n^b - \theta_m^a), \tag{13}$$

where $a, b = \mathrm{A}, \mathrm{B}$ represent the two communities and m labels the oscillators. The coupling constants J_{mn} can be J_{AA}, J_{AB}, J_{BA}, J_{BB} depending on which populations the oscillators m and n belong to, and the conventional Kuramoto model[33,224] is recovered by setting the coupling strengths to be identical, that is, $J_{\mathrm{AA}} = J_{\mathrm{AB}} = J_{\mathrm{BA}} = J_{\mathrm{BB}}$. In Supplementary Information section IX, we derive a self-consistency equation for the steady state, which ends up being very similar to equation (11) (with $\partial_t \to \mathrm{i}\Omega$). To analyse the dynamics of the system and the stability of the solutions, we now focus on the (exact) mean-field dynamics in the case of Lorentzian frequency distributions for each community.

The dynamics of the generalized Kuramoto model in equation (13) can exactly be captured by a small number of coupled differential equations in the limit of a large number of oscillators; see refs. [12,135,229,230,232,236–242] and the review ref. [243]. In Supplementary Information section IX, we confirm that this mean-field dynamics is quantitatively consistent with direct simulations of the microscopic model equation (2).

Following Kuramoto[224], we introduce the order parameters

$$z_a(t) = \frac{1}{N_a} \sum_{m=1}^{N_a} \mathrm{e}^{\mathrm{i}\theta_m^a(t)}, \tag{14}$$

which become finite when the oscillators synchronize. The amplitude and the phase of $z_a(t)$ characterize, respectively, the phase coherence and the average phase of the component a.

Through the mean-field reduction, the evolution of the complex order parameter $z_a(t)$ for each community a is described by[230]

$$\partial_t z_a = (\mathrm{i}\omega_a - \Delta_a) z_a + \frac{1}{2} \sum_b j_{ab} (z_b - z_a^2 \bar{z}_b), \tag{15}$$

where $\bar{z}_b$ is the complex conjugate of z_b, and where we have defined $j_{ab} = J_{ab} N_b$. We have assumed that the natural frequencies of the oscillators in the community a follow a Lorentzian distribution $g_a(\omega) = \pi^{-1}[(\omega - \omega_a)^2 + \Delta_a^2]^{-1}$. The term $\mathrm{i}\omega_a z_a$ in equation (15) explicitly breaks the mirror symmetry $z_a \to \bar{z}_a$ (and hence parity, which here corresponds to the generalized PT symmetry), but is invariant under rotations $z_a \to \mathrm{e}^{\mathrm{i}\theta} z_a$.

When $\omega_a = 0$ for all the communities, the system has a full O(2) symmetry, and one observes phases with spontaneously broken parity. In this paragraph, we focus on this situation. To mirror the analysis in the main text, we define $j_\pm = (j_{\mathrm{AB}} \pm j_{\mathrm{BA}})/2$ and determine a numerical phase diagram of the system in the (j_-, j_+) plane; see Extended Data Fig. 4. This phase diagram shares several qualitative features with the flocking phase diagram in Fig. 2. In particular, we find that the phase boundaries between the (anti)synchronized state (labelled coherent and π state in Extended Data Fig. 4) and the chiral state (labelled travelling wave in Extended Data Fig. 4) are marked by exceptional points in the Jacobian L of the dynamical system equation (15). Writing the right-hand side of equation (15) as $f_a(z_b)$, the 4×4 Jacobian matrix L has blocks

$$L_{ab} = \begin{pmatrix} \partial f_b / \partial z_a & \partial f_b / \partial \bar{z}_a \\ \partial \bar{f}_b / \partial z_a & \partial \bar{f}_b / \partial \bar{z}_a \end{pmatrix} \tag{16}$$

for $a, b = \mathrm{A}, \mathrm{B}$, where the derivatives are evaluated at the steady state. A direct numerical evaluation of this matrix shows that the two most unstable eigenvalues indeed coalesce (that is, form an exceptional point) at the transition; see Extended Data Fig. 4 for an example.

The similarity between Extended Data Fig. 4 and Fig. 2 can be anticipated: the Vicsek model is, in essence, an extension of the Kuramoto model in which the oscillators move (besides several differences in their most common incarnations). A finite natural frequency $\omega_{\mathrm{A}} = \omega_{\mathrm{B}} \equiv \omega_0 \neq 0$ common to all communities can be removed by a transformation of the degrees of freedom (where the oscillators are observed in a rotating frame).

To analyse the situation with explicitly broken PT symmetry (class II), we introduce a finite detuning $\Delta\omega = \omega_{\mathrm{A}} - \omega_{\mathrm{B}}$ between the natural frequencies of the two communities (we keep $\omega_{\mathrm{A}} + \omega_{\mathrm{B}} = 0$ for simplicity). In this case, exceptional points occur at points in a two-dimensional parameter space (their codimension is two). This is consistent with the occurrence of Bogdanov–Takens points in generalized Kuramoto models[228,233–235,244,245], in which hysteresis can be present[244,245].

The numerical simulation of equation (15) shows that there are regions of the phase diagram in which two states (clockwise and anticlockwise) coexist, as well as regions in which a single state is present. This can be understood as the result between the spontaneous PT-symmetry breaking at $\Delta\omega = 0$ (in which the two states are equivalent, and mapped to each other by PT symmetry) and the detuning that explicitly breaks PT symmetry (see Supplementary Information section III for a discussion on PT symmetry). At the boundary between these regions, the properties of the steady states (such as their frequency $\Omega_{\mathrm{ss}} \equiv \Omega$) change in a discontinuous way (such as in a first-order phase transition). This is illustrated in Extended Data Fig. 5. In Extended Data Fig. 5a, we show the manifold of stable steady states obtained from numerical simulations, which is a truncated version of the Riemann surface of the square root characteristic of exceptional points. There is coexistence between

two states (blue and red dots) in the red region in parameter space. In Extended Data Fig. 5b, we show hysteresis curves corresponding to slices of the manifold represented in Extended Data Fig. 5a.

This behaviour shares some features with the dynamical encircling of an exceptional point in a linear system[246–249]. However, a crucial difference is that here, we are dealing with the steady state (that is, many-body phase) of the system, which is possible only because of the nonlinearity (similar situations occur in refs. [30,50,250–255]). In addition, the breakdown of the adiabatic theorem plays a crucial role in the situations analysed in refs. [246–249], but it is not the case in the first-order-like transitions and hysteretic behaviour described here. In particular, the hysteresis observed in Extended Data Fig. 5 does not depend on the speed at which the parameters are changed ($\Delta\omega$ in Extended Data Fig. 5b), provided that the change is slow enough (so that the system is always in a steady state). The hysteresis curve is then independent of the arbitrarily small rate of change. This is in sharp contrast with the situations analysed in refs. [246–249]. These are ruled by a linear dynamical system, in which the most unstable state (that is, the one with the largest positive growth rate) always eventually dominates given enough time. In this situation, there is no hysteresis in the limit of an arbitrarily small rate of change.

Non-reciprocal pattern-forming instabilities

In this section, we apply our general strategy to pattern-forming instabilities within the formalism of amplitude equations[40,66,67,256–258]. These describe a variety of physical systems ranging from fluid convection and lasers to ecological and chemical reaction-diffusion systems.

To clear any misunderstanding, let us warn the reader: this section is not about the exceptional-point-enforced pattern formation in Fig. 3. Instead, we consider non-reciprocal pattern formation, in which two fields are coupled in a non-reciprocal way. Here, the pattern formation is the spontaneous symmetry breaking (the Euclidean group E(d) of isometries of space is broken by the appearance of the pattern), and the pattern starts travelling at the (anti)aligned–chiral transition.

We first reinterpret equation (1) as an amplitude equation for the complex amplitude $A_a \equiv v_a^x + \mathrm{i}v_a^y$. Correspondingly, we perform direct simulations of the toy model equation (4), describing two coupled copies of the Swift–Hohenberg equation[259], a simple model of pattern formation.

We then discuss a slightly more complicated situation, in which a single physical field is present, but two Fourier modes with non-reciprocal couplings are relevant (the non-reciprocity occurs between the harmonics), in which patterns with spontaneously broken parity also occur[13,14,260–264] (see also refs. [265–268]). This situation has several experimental realizations in directional solidification of liquid crystals[42,269–271], directional solidification of lamellar eutectics[43,272–274], directional viscous fingering[15,41,275,276] and in overflowing fountains[44,277]. We show that in this situation too, the transition is marked by an exceptional point where the Goldstone mode of the spontaneously broken translation symmetry (phase diffusion) coalesces with a damped mode.

Without any attempt at completeness, we also refer to refs. [278–291] on binary convection and to refs. [292–299] on the visual cortex, and to refs. [300–308] on Taylor–Couette/Dean flows.

Coupled amplitude equations. Let us first consider the one-dimensional Ginzburg–Landau amplitude equation

$$\partial_t A = \epsilon A - g|A|^2 A + D\partial_x^2 A, \tag{17}$$

where A is a complex amplitude. This equation describes, for instance, rolls in Rayleigh–Bénard convection. The physical field u (such as velocity or temperature) reads $u(t,x) = A(t,x)\mathrm{e}^{\mathrm{i}(q_c x)} + \mathrm{c.c.}$, where q_c is the wavenumber of the convection rolls, and $A(t,x)$ is a slowly varying envelope. The apparition of a pattern is marked by $A \neq 0$, and corresponds to the spontaneous breaking of translation symmetry. The amplitude equation (17) satisfies translation symmetry by which $A \to A\mathrm{e}^{\mathrm{i}\phi}$, corresponding to a translation of the pattern by a distance ϕ/q_c in the x direction; as well as inversion symmetry $x \to -x$ by which $A \to \overline{A}$ (overbar is complex conjugation). The reflection does not commute with the translations, so overall we do not have the direct product of these groups, but instead the semidirect product $U(1) \rtimes Z_2 \cong \mathrm{O}(2)$ (where $\cong$ indicates a group isomorphism). This symmetry prohibits terms such as A^2 in the right-hand side of equation (17), and guarantees that the coefficients are real.

Let us now introduce non-reciprocity: to do so, we consider two coupled amplitudes A_1 and A_2 (describing two different coupled fields), and write the most general equation of motion compatible with the symmetry, up to third order (like in equation (17)). The only terms allowed are first order terms, as well as third order terms of the form $(\overline{A}_b A_c + \overline{A}_c A_b)A_d$, in both cases with real coefficients. Hence, our amplitude equation reads

$$\partial_t A_a = \epsilon_{ab} A_b - g_{abcd}(\overline{A}_b A_c + \overline{A}_c A_b)A_d + D_{ab}\partial_x^2 A_b, \tag{18}$$

where all the coefficients are real. Focusing on spatially uniform amplitudes and ignoring diffusive terms in equation (18), we recognize equation (1) upon representing the complex amplitude A_a as a two-dimensional $v_a = (\mathrm{Re}A_a, \mathrm{Im}A_a)$, owing to the fact that the symmetry groups are isomorphic. We note, however, that the physical interpretation of the symmetries are different in both cases. Having identified equation (18) with equation (1) (in the uniform case), we can immediately predict that all the phases described in the main text for flocking should exist here (see Extended Data Fig. 6 for their interpretation in this context).

Our analysis focused on the mean-field ($k = 0$) transitions, and our conclusions remain valid as long as the growth rates are negative at finite k (this is, in particular, the case where $D_{ab} = D\delta_{ab}$, where δ_{ab} is the Kronecker delta, so the growth rates are of the form $\sigma_i(k) = \sigma_i(0) - Dk^2$; but this is especially not guaranteed when D_{ab} is not symmetric). We emphasize that we did not assume non-reciprocal cross-diffusion, in contrast with refs. [55,56] (another difference with these references is that we consider a non-conserved order parameter in the language of ref. [32]).

We also mention that upon lifting the constraint put upon equation (18) by reflection symmetry, one is left with a U(1)-equivariant system with explicitly broken PT symmetry (see Supplementary Information section III for definitions and discussions, including refs. [25,106–115]), and equation (18) becomes a complex Ginzburg–Landau equation. We expect the analysis of Methods section 'Non-reciprocal Kuramoto model' to apply in this case.

Coupled Swift–Hohenberg equations. To further support our claims and illustrate the phases described above, we consider two coupled Swift–Hohenberg equations in equation (4) describing the dynamics of the real fields $u_a(t,x)$, with $a = 1, 2$ (we also define $r_\pm = (r_{12} \pm r_{21})/2$). An explicit version of the amplitude equations (18) (obtained from symmetry considerations) could be derived from equation (4), following for example, ref. [66]. Instead, we solve equation (4) numerically on a one-dimensional domain of size $2L$ with periodic boundary conditions using the open-source pseudospectral solver Dedalus[219], starting from random initial conditions. The results confirm our predictions based on the coupled amplitude equations (18). In Extended Data Fig. 6, we show snapshots of the numerical results, in which all the phases described above appear. In this case, equation (4) has the full Euclidean group E(1) as a symmetry group, which is broken by pattern formation. (The O(2) symmetry of equation (18) pertains to the amplitude equation description, in which additional knowledge about the pattern is taken into account.)

Directional interface growth. Following refs. [13,14,262–264], we now consider a single scalar field decomposed as

$$u(t,x) = A_1(t,x)\mathrm{e}^{\mathrm{i}(q_c x)} + A_2(t,x)\mathrm{e}^{\mathrm{i}2(q_c x)} + \mathrm{c.c.} \tag{19}$$

As in the previous case, the transition and reflection symmetry of the underlying system endows the amplitude equation with O(2) symmetry. However, note that while A_1 transforms as $A_1 \to A_1 e^{i\theta}$ when the field u is translated in space, A_2 transforms as $A_2 \to A_2 e^{2i\theta}$. This is a different representation of the SO(2) group compared to the previous paragraph. (The $\mathbb{Z}_2$ part is unchanged, and still corresponds to $A_1 \to \bar{A}_1$ and $A_2 \to \bar{A}_2$.) Because the representation is different, the general form of the amplitude is different, and reads[13,14,262–264]

$$\begin{aligned} \partial_t A_1 &= \mu_1 A_1 - \bar{A}_1 A_2 - \alpha|A_1|^2 A_1 - \beta|A_2|^2 A_1, \\ \partial_t A_2 &= \mu_2 A_2 + \epsilon A_1^2 - \gamma|A_1|^2 A_2 - \delta|A_2|^2 A_2. \end{aligned} \tag{20}$$

The coefficients α, β, γ and δ are usually assumed to be positive to ensure stability, and the coefficient of $\bar{A}_1 A_2$ is set to −1 by rescaling. The non-reciprocity is then captured by the coefficient ϵ being positive, which is necessary for the apparition of travelling patterns[262]. As the amplitudes $A_1 = r_1 e^{i\phi_1}$ and $A_2 = r_2 e^{i\phi_2}$ correspond to different Fourier components, the relevant phase difference between them is $\Delta\phi = 2\phi_1 - \phi_2$.

In Extended Data Fig. 7, we show the spectrum of the operator L obtained by linearizing equation (20) around its steady state (see equation (16) for the definition of L, with the replacement $z_a \to A_a$). At the transition between a static solution (representing a static pattern) and a travelling-wave solution (representing a travelling pattern), we observe the coalescence of the Goldstone mode with a damped mode at an exceptional point (red circle in the figure). We also note that the presence of exceptional points away from zero in the spectrum of L does not mark a phase transition (bifurcation).

Data availability

No data were generated during the course of this study.

Code availability

The computer code used in this study is available on Zenodo at https://doi.org/10.5281/zenodo.4605984 under the 2-clause BSD licence.

57. Landau, L. & Khalatnikov, I. On the anomalous absorption of sound near a second-order phase transition point. *Dokl. Akad. Nauk SSSR* **96**, 469–472 (1954).
58. Cugliandolo, L. F. & Kurchan, J. Weak ergodicity breaking in mean-field spin-glass models. *Philos. Mag. B* **71**, 501–514 (1995).
59. Keim, N. C., Paulsen, J. D., Zeravcic, Z., Sastry, S. & Nagel, S. R. Memory formation in matter. *Rev. Mod. Phys*. **91**, 035002 (2019).
60. Van Hove, L. Time-dependent correlations between spins and neutron scattering in ferromagnetic crystals. *Phys. Rev*. **95**, 1374–1384 (1954).
61. Hohenberg, P. & Krekhov, A. An introduction to the Ginzburg–Landau theory of phase transitions and nonequilibrium patterns. *Phys. Rep*. **572**, 1–42 (2015).
62. Wilson, K. The renormalization group and the epsilon expansion. *Phys. Rep*. **12**, 75–199 (1974).
63. Laguës, M. & Lesne, A. *Invariances d'Échelle: des Changements d'États à la Turbulence* (Belin, 2003).
64. Muñoz, M. A. Criticality and dynamical scaling in living systems. *Rev. Mod. Phys*. **90**, 031001 (2018).
65. Sornette, D. *Critical Phenomena in Natural Sciences* (Springer, 2000).
66. van Saarloos, W. The complex Ginzburg–Landau equation for beginners. *Spatio-temporal Patterns in Nonequilibrium Complex Systems* Vol. XXI (eds Cladis, P. E. & Palffy-Muhoray, P.) (Addison-Wesley, 1994).
67. Aranson, I. S. & Kramer, L. The world of the complex Ginzburg–Landau equation. *Rev. Mod. Phys*. **74**, 99–143 (2002).
68. Golubitsky, M. & Schaeffer, D. G. *Singularities and Groups in Bifurcation Theory* Vol. I (Springer, 1985).
69. Golubitsky, M., Stewart, I. & Schaeffer, D. G. *Singularities and Groups in Bifurcation Theory* Vol. II (Springer, 1988).
70. Crawford, J. D. & Knobloch, E. Symmetry and symmetry-breaking bifurcations in fluid dynamics. *Annu. Rev. Fluid Mech*. **23**, 341–387 (1991).
71. Chossat, P. & Lauterbach, R. *Methods in Equivariant Bifurcations and Dynamical Systems* (World Scientific, 2000).
72. Haken, H. (ed.) *Synergetics* (Springer, 1977).
73. Henkel, M., Hinrichsen, H. & Lübeck, S. *Non-equilibrium Phase Transitions* Vol. 1 (Springer, 2008).
74. Henkel, M. & Pleimling, M. *Non-equilibrium Phase Transitions* Vol. 2 (Springer, 2010).
75. Livi, R. & Politi, P. *Nonequilibrium Statistical Physics: A Modern Perspective* (Cambridge Univ. Press, 2017).
76. Aron, C. & Chamon, C. Landau theory for non-equilibrium steady states, *SciPost Phys*. **8**, 074 (2020).
77. Marchetti, M. C. et al. Hydrodynamics of soft active matter. *Rev. Mod. Phys*. **85**, 1143 (2013).
78. Trefethen, L. N. & Embree, M. *Spectra and Pseudospectra* (Princeton Univ. Press, 2005).
79. Böberg, L. & Brosa, U. Onset of turbulence in a pipe. *Z. Naturforsch. A* **43**, 697–726 (1988).
80. Farrell, B. F. & Ioannou, P. J. Variance maintained by stochastic forcing of non-normal dynamical systems associated with linearly stable shear flows. *Phys. Rev. Lett*. **72**, 1188–1191 (1994).
81. Dauchot, O. & Manneville, P. Local versus global concepts in hydrodynamic stability theory. *J. Phys. II* **7**, 371–389 (1997).
82. Grossmann, S. The onset of shear flow turbulence. *Rev. Mod. Phys*. **72**, 603–618 (2000).
83. Chomaz, J.-M. Global instabilities in spatially developing flows: non-normality and nonlinearity. *Annu. Rev. Fluid Mech*. **37**, 357–392 (2005).
84. Wu, J.-Z., Ma, H.-Y. & Zhou, M.-D. *Vorticity And Vortex Dynamics* (Springer, 2006).
85. Schmid, P. J. Nonmodal stability theory. *Annu. Rev. Fluid Mech*. **39**, 129–162 (2007).
86. Kerswell, R. Nonlinear nonmodal stability theory. *Annu. Rev. Fluid Mech*. **50**, 319–345 (2018).
87. Chajwa, R., Menon, N., Ramaswamy, S. & Govindarajan, R. Waves, algebraic growth, and clumping in sedimenting disk arrays. *Phys. Rev. X* **10**, 041016 (2020).
88. Murphy, B. K. & Miller, K. D. Balanced amplification: a new mechanism of selective amplification of neural activity patterns. *Neuron* **61**, 635–648 (2009); correction **89**, 235 (2016).
89. Hennequin, G., Vogels, T. P. & Gerstner, W. Non-normal amplification in random balanced neuronal networks. *Phys. Rev. E* **86**, 011909 (2012).
90. Amir, A., Hatano, N. & Nelson, D. R. Non-Hermitian localization in biological networks. *Phys. Rev. E* **93**, 042310 (2016).
91. Asllani, M. & Carletti, T. Topological resilience in non-normal networked systems. *Phys. Rev. E* **97**, 042302 (2018).
92. Asllani, M., Lambiotte, R. & Carletti, T. Structure and dynamical behavior of non-normal networks. *Sci. Adv*. **4**, eaau9403 (2018).
93. Baggio, G., Rutten, V., Hennequin, G. & Zampieri, S. Efficient communication over complex dynamical networks: the role of matrix non-normality. *Sci. Adv*. **6**, eaba2282 (2020).
94. Nicolaou, Z. G., Nishikawa, T., Nicholson, S. B., Green, J. R. & Motter, A. E. Non-normality and non-monotonic dynamics in complex reaction networks. *Phys. Rev. Res*. **2**, 043059 (2020).
95. Neubert, M. G. & Caswell, H. Alternatives to resilience for measuring the responses of ecological systems to perturbations. *Ecology* **78**, 653–665 (1997).
96. Nelson, D. R. & Shnerb, N. M. Non-Hermitian localization and population biology. *Phys. Rev. E* **58**, 1383 (1998).
97. Neubert, M. G., Klanjscek, T. & Caswell, H. Reactivity and transient dynamics of predator–prey and food web models. *Ecol. Modell*. **179**, 29 (2004).
98. Townley, S., Carslake, D., Kellie-smith, O., Mccarthy, D. & Hodgson, D. Predicting transient amplification in perturbed ecological systems. *J. Appl. Ecol*. **44**, 1243 (2007).
99. Ridolfi, L., Camporeale, C., D'Odorico, P. & Laio, F. Transient growth induces unexpected deterministic spatial patterns in the Turing process. *Europhys. Lett*. **95**, 18003 (2011).
100. Feng, L., El-Ganainy, R. & Ge, L. Non-Hermitian photonics based on parity–time symmetry. *Nat. Photon*. **11**, 752 (2017).
101. Makris, K., Ge, L. & Türeci, H. Anomalous transient amplification of waves in non-normal photonic media. *Phys. Rev. X* **4**, 041044 (2014).
102. Ashida, Y., Gong, Z. & Ueda, M. Non-Hermitian physics. Preprint at https://arxiv.org/abs/2006.01837 (2020).
103. Tripathi, V., Galda, A., Barman, H. & Vinokur, V. M. Parity–time symmetry-breaking mechanism of dynamic Mott transitions in dissipative systems. *Phys. Rev. B* **94**, 041104 (2016).
104. Bernier, N. R., Torre, E. G. D. & Demler, E. Unstable avoided crossing in coupled spinor condensates. *Phys. Rev. Lett*. **113**, 065303 (2014).
105. Aharonyan, M. & Torre, E. G. D. Many-body exceptional points in colliding condensates. *Mol. Phys*. **117**, 1971 (2019).
106. Mostafazadeh, A. Pseudo-Hermiticity versus PT symmetry: the necessary condition for the reality of the spectrum of a non-Hermitian Hamiltonian. *J. Math. Phys*. **43**, 205 (2002).
107. Mostafazadeh, A. Pseudo-Hermiticity versus PT-symmetry. II: A complete characterization of non-Hermitian Hamiltonians with a real spectrum. *J. Math. Phys*. **43**, 2814 (2002).
108. Mostafazadeh, A. Pseudo-Hermiticity versus PT-symmetry. III: Equivalence of pseudo-Hermiticity and the presence of antilinear symmetries. *J. Math. Phys*. **43**, 3944 (2002).
109. Bender, C. M., Berry, M. V. & Mandilara, A. Generalized PT symmetry and real spectra. *J. Phys. Math. Gen*. **35**, L467 (2002).
110. Bender, C. M. & Mannheim, P. D. PT symmetry and necessary and sufficient conditions for the reality of energy eigenvalues. *Phys. Lett. A* **374**, 1616–1620 (2010).
111. Mostafazadeh, A. Physics of spectral singularities. In *Trends in Mathematics* (eds Kielanowski, P. et al.) 145–165 (Springer, 2015).
112. Bender, C. M. Making sense of non-Hermitian Hamiltonians. *Rep. Prog. Phys*. **70**, 947 (2007).
113. Weigert, S. PT-symmetry and its spontaneous breakdown explained by anti-linearity. *J. Opt. B* **5**, S416 (2003).
114. Wigner, E. P. Normal form of antiunitary operators. *J. Math. Phys*. **1**, 409 (1960).
115. Konotop, V. V., Yang, J. & Zezyulin, D. A. Nonlinear waves in PT-symmetric systems. *Rev. Mod. Phys*. **88**, 035002 (2016).
116. van Kampen, N. G. *Stochastic Processes in Physics and Chemistry* Vol. 1 (Elsevier, 2007).
117. Risken, H. *The Fokker–Planck Equation* (Springer, 1989).
118. Gardiner, C. W. *Handbook of Stochastic Methods* (Springer, 2004).
119. Lan, G., Sartori, P., Neumann, S., Sourjik, V. & Tu, Y. The energy–speed–accuracy trade-off in sensory adaptation. *Nat. Phys*. **8**, 422 (2012).

120. Weiss, J. B. Coordinate invariance in stochastic dynamical systems. *Tellus* **A55**, 208–218 (2003).
121. Newton, I. *Philosophiæ Naturalis Principia Mathematica* (1687).
122. Ermak, D. L. & McCammon, J. A. Brownian dynamics with hydrodynamic interactions. *J. Chem. Phys.* **69**, 1352 (1978).
123. Di Leonardo, R. et al. Hydrodynamic interactions in two dimensions. *Phys. Rev. E* **78**, 031406 (2008).
124. Lahiri, R., Barma, M. & Ramaswamy, S. Strong phase separation in a model of sedimenting lattices. *Phys. Rev. E* **61**, 1648 (2000).
125. Kryuchkov, N. P., Ivlev, A. V. & Yurchenko, S. O. Dissipative phase transitions in systems with nonreciprocal effective interactions. *Soft Matter* **14**, 9720 (2018).
126. Soto, R. & Golestanian, R. Self-assembly of catalytically active colloidal molecules: tailoring activity through surface chemistry. *Phys. Rev. Lett.* **112**, 068301 (2014).
127. Agudo-Canalejo, J. & Golestanian, R. Active phase separation in mixtures of chemically interacting particles. *Phys. Rev. Lett.* **123**, 018101 (2019).
128. Dholakia, K. & Zemánek, P. Gripped by light: optical binding. *Rev. Mod. Phys.* **82**, 1767–1791 (2010).
129. Yifat, Y. D. et al. Reactive optical matter: light-induced motility in electrodynamically asymmetric nanoscale scatterers. *Light Sci. Appl.* **7**, 105 (2018).
130. Peterson, C. W., Parker, J., Rice, S. A. & Scherer, N. F. Controlling the dynamics and optical binding of nanoparticle homodimers with transverse phase gradients. *Nano Lett.* **19**, 897–903 (2019).
131. Krakauer, J. W., Ghazanfar, A. A., Gomez-Marin, A., MacIver, M. A. & Poeppel, D. Neuroscience needs behavior: correcting a reductionist bias. *Neuron* **93**, 480 (2017).
132. Parisi, G. Asymmetric neural networks and the process of learning. *J. Phys. Math. Gen.* **19**, L675 (1986).
133. Derrida, B., Gardner, E. & Zippelius, A. An exactly solvable asymmetric neural network model. *Europhys. Lett.* **4**, 167 (1987).
134. Dayan, P. & Abbott, L. *Theoretical Neuroscience: Computational and Mathematical Modelling of Neural Systems* (MIT Press, 2001).
135. Hong, H. & Strogatz, S. H. Conformists and contrarians in a Kuramoto model with identical natural frequencies. *Phys. Rev. E* **84**, 046202 (2011).
136. Pluchino, A., Latora, V. & Rapisarda, A. Changing opinions in a changing world: a new perspective in sociophysics. *Int. J. Mod. Phys. C* **16**, 515 (2005).
137. Morin, A., Caussin, J.-B., Eloy, C. & Bartolo, D. Collective motion with anticipation: flocking, spinning, and swarming. *Phys. Rev. E* **91**, 012134 (2015).
138. Ginelli, F. et al. Intermittent collective dynamics emerge from conflicting imperatives in sheep herds. *Proc. Natl Acad. Sci. USA* **112**, 12729 (2015).
139. Dadhichi, L. P., Kethapelli, J., Chajwa, R., Ramaswamy, S. & Maitra, A. Nonmutual torques and the unimportance of motility for long-range order in two-dimensional flocks. *Phys. Rev. E* **101**, 052601 (2020).
140. Barberis, L. & Peruani, F. Large-scale patterns in a minimal cognitive flocking model: incidental leaders, nematic patterns, and aggregates. *Phys. Rev. Lett.* **117**, 248001 (2016).
141. Gupta, R. K., Kant, R., Soni, H., Sood, A. K. & Ramaswamy, S. Active nonreciprocal attraction between motile particles in an elastic medium. Preprint at https://arxiv.org/abs/2007.04860 (2020).
142. Maitra, A., Lenz, M. & Voituriez, R. Chiral active hexatics: giant number fluctuations, waves and destruction of order. *Phys. Rev. Lett.* **125**, 238005 (2020).
143. Durve, M., Saha, A. & Sayeed, A. Active particle condensation by non-reciprocal and time-delayed interactions. *Eur. Phys. J. E* **41**, 49 (2018).
144. Costanzo, A. Milling-induction and milling-destruction in a Vicsek-like binary-mixture model. *Europhys. Lett.* **125**, 20008 (2019).
145. Lin, Z. et al. Unidirectional invisibility induced by PT-symmetric periodic structures. *Phys. Rev. Lett.* **106**, 213901 (2011).
146. Coulais, C., Sounas, D. & Alù, A. Static non-reciprocity in mechanical metamaterials. *Nature* **542**, 461 (2017).
147. Ghatak, A., Brandenbourger, M., van Wezel, J. & Coulais, C. Observation of non-Hermitian topology and its bulk–edge correspondence in an active mechanical metamaterial. *Proc. Natl Acad. Sci. USA* **117**, 29561 (2020).
148. Rosa, M. I. N. & Ruzzene, M. Dynamics and topology of non-Hermitian elastic lattices with non-local feedback control interactions. *New J. Phys.* **22**, 053004 (2020).
149. Chen, Y., Li, X., Scheibner, C., Vitelli, V. & Huang, G. Self-sensing metamaterials with odd micropolarity. Preprint at https://arxiv.org/abs/2009.07329 (2020).
150. Das, J., Rao, M. & Ramaswamy, S. Nonequilibrium steady states of the isotropic classical magnet. Preprint at https://arxiv.org/abs/cond-mat/0404071 (2004).
151. Tasaki, H. Hohenberg–Mermin–Wagner-type theorems for equilibrium models of flocking. *Phys. Rev. Lett.* **125**, 220601 (2020).
152. Fodor, É. et al. How far from equilibrium is active matter? *Phys. Rev. Lett.* **117**, 038103 (2016).
153. Loos, S. A. M. & Klapp, S. H. L. Thermodynamic implications of non-reciprocity. Preprint at https://arxiv.org/abs/2008.00894 (2020).
154. Loos, S. A. M., Hermann, S. M. & Klapp, S. H. L. Non-reciprocal hidden degrees of freedom: a unifying perspective on memory, feedback, and activity. Preprint at https://arxiv.org/abs/1910.08372 (2019).
155. Malzard, S., Poli, C. & Schomerus, H. Topologically protected defect states in open photonic systems with non-Hermitian charge conjugation and parity–time symmetry. *Phys. Rev. Lett.* **115**, 200402 (2015).
156. Lee, C. H. & Thomale, R. Anatomy of skin modes and topology in non-Hermitian systems. *Phys. Rev. B* **99**, 201103 (2019).
157. Lee, C. H., Li, L., Thomale, R. & Gong, J. Unraveling non-Hermitian pumping: emergent spectral singularities and anomalous responses. *Phys. Rev. B* **102**, 085151 (2020).
158. Okuma, N., Kawabata, K., Shiozaki, K. & Sato, M. Topological origin of non-Hermitian skin effects. *Phys. Rev. Lett.* **124**, 086801 (2020).
159. Hofmann, T., Helbig, T., Lee, C. H., Greiter, M. & Thomale, R. Chiral voltage propagation and calibration in a topolectrical Chern circuit. *Phys. Rev. Lett.* **122**, 247702 (2019).
160. Lee, C. H., Li, L. & Gong, J. Hybrid higher-order skin-topological modes in nonreciprocal systems. *Phys. Rev. Lett.* **123**, 016805 (2019).
161. Zhang, K., Yang, Z. & Fang, C. Correspondence between winding numbers and skin modes in non-Hermitian systems. *Phys. Rev. Lett.* **125**, 126402 (2020).
162. Achenbach, J. D. *Reciprocity in Elastodynamics* (Cambridge Univ. Press, 2004).
163. Nassar, H. et al. Nonreciprocity in acoustic and elastic materials. *Nat. Rev. Mater.* (2020).
164. Potton, R. J. Reciprocity in optics. *Rep. Prog. Phys.* **67**, 717 (2004).
165. Estep, N. A., Sounas, D. L., Soric, J. & Alù, A. Magnetic-free non-reciprocity and isolation based on parametrically modulated coupled-resonator loops. *Nat. Phys.* **10**, 923 (2014).
166. Caloz, C. et al. Electromagnetic nonreciprocity. *Phys. Rev. Appl.* **10**, 047001 (2018).
167. Masoud, H. & Stone, H. A. The reciprocal theorem in fluid dynamics and transport phenomena. *J. Fluid Mech.* **879**, P1 (2019).
168. Scheibner, C., Irvine, W. T. M. & Vitelli, V. Non-Hermitian band topology and skin modes in active elastic media. *Phys. Rev. Lett.* **125**, 118001 (2020).
169. Zhou, D. & Zhang, J. Non-Hermitian topological metamaterials with odd elasticity. *Phys. Rev. Res.* **2**, 023173 (2020).
170. Groot, S. R. D. & Mazur, P. *Non-Equilibrium Thermodynamics* (Dover Publications, 1962).
171. Maltman, K. & Laidlaw, W. G. Onsager symmetry and the diagonalizability of the hydrodynamic matrix. *J. Math. Phys.* **16**, 1561 (1975).
172. Avron, J. E. Odd viscosity. *J. Stat. Phys.* **92**, 543–557 (1998).
173. Banerjee, D., Souslov, A., Abanov, A. G. & Vitelli, V. Odd viscosity in chiral active fluids. *Nat. Commun.* **8**, 1573 (2017).
174. Souslov, A., Dasbiswas, K., Fruchart, M., Vaikuntanathan, S. & Vitelli, V. Topological waves in fluids with odd viscosity. *Phys. Rev. Lett.* **122**, 128001 (2019).
175. Soni, V. et al. The odd free surface flows of a colloidal chiral fluid. *Nat. Phys.* **15**, 1188–1194 (2019).
176. Han, M. et al. Statistical mechanics of a chiral active fluid. Preprint at https://arxiv.org/abs/2002.07679 (2020).
177. Arnold, V. I. *Geometrical Methods in the Theory of Ordinary Differential Equations* (Springer, 1988).
178. Bogdanov, R. I. Bifurcations of a limit cycle for a family of vector fields on the plane. *Selecta Math. Sov.* **1**, 373 (1981); translated from *Trudy Sem. Petrovsk.* **2**, 23–35 (1976).
179. Bogdanov, R. I. Versal deformations of a singularity of a vector field on the plane in the case of zero eigenvalues. *Selecta Math. Sov.* **1**, 389 (1981); translated from *Trudy Sem. Petrovsk.* **2**, 37–65 (1976).
180. Takens, F. in *Global Analysis of Dynamical Systems* (eds Broer, H. W. et al.) 1–63 (IOP, 2001); reprinted from *Commun. Math. Inst. Rijksuniv. Utrecht* **2**, 1–111 (1974).
181. Nambu, Y. Quasi-particles and gauge invariance in the theory of superconductivity. *Phys. Rev.* **117**, 648 (1960).
182. Goldstone, J. Field theories with superconductor solutions. *Nuovo Cim.* **19**, 154–164 (1961).
183. Goldstone, J., Salam, A. & Weinberg, S. Broken symmetries. *Phys. Rev.* **127**, 965 (1962).
184. Hidaka, Y. Counting rule for Nambu–Goldstone modes in nonrelativistic Systems. *Phys. Rev. Lett.* **110**, 091601 (2013).
185. Watanabe, H. Counting rules of Nambu–Goldstone modes. *Annu. Rev. Condens. Matter Phys.* **11**, 169 (2020).
186. Watanabe, H. & Murayama, H. Unified description of Nambu–Goldstone bosons without Lorentz invariance. *Phys. Rev. Lett.* **108**, 251602 (2012).
187. Nielsen, H. & Chadha, S. On how to count Goldstone bosons. *Nucl. Phys. B* **105**, 445 (1976).
188. Leroy, L. On spontaneous symmetry breakdown in dynamical systems. *J. Phys. Math. Gen.* **25**, L987 (1992).
189. Minami, Y. & Hidaka, Y. Spontaneous symmetry breaking and Nambu–Goldstone modes in dissipative systems. *Phys. Rev. E* **97**, 012130 (2018).
190. Hongo, M., Kim, S., Noumi, T. & Ota, A. Effective Lagrangian for Nambu–Goldstone modes in nonequilibrium open systems. Preprint at https://arxiv.org/abs/1907.08609 (2019).
191. Von Neumann, J. & Wigner, E. P. Über das Verhalten von Eigenwerten bei adiabatischen Prozessen *Physik. Zeit.* **30**, 467 (1929); translated in *Symmetry in the Solid State* (eds Knox, R. S. & Gold, A.) (Benjamin, New York, 1964).
192. Arnold, V. I. Modes and quasimodes. *Funct. Anal. Appl.* **6**, 94 (1972); translated from *Funktsional. Anal. i Prilozhen.* **6**, 12–20 (1972).
193. Arnold, V. I. Remarks on eigenvalues and eigenvectors of Hermitian matrices, Berry phase, adiabatic connections and quantum Hall effect. *Selecta Mathematica* **1**, 1–19 (1995).
194. Seyranian, A. P., Kirillov, O. N. & Mailybaev, A. A. Coupling of eigenvalues of complex matrices at diabolic and exceptional points. *J. Phys. Math. Gen.* **38**, 1723 (2005).
195. Julien, K. A. Strong spatial interactions with 1:1 resonance: a three-layer convection problem. *Nonlinearity* **7**, 1655 (1994).
196. Renardy, Y. Y., Renardy, M. & Fujimura, K. Takens–Bogdanov bifurcation on the hexagonal lattice for double-layer convection. *Physica D* **129**, 171 (1999).
197. Guckenheimer, J. A codimension two bifurcation with circular symmetry. In *Multiparameter Bifurcation Theory* (eds Golubitsky, M. & Guckenheimer, J. M.) 175–184 (AMS, 1986).
198. Dangelmayr, G. & Knobloch, E. The Takens–Bogdanov bifurcation with O(2) symmetry. *Phil. Trans. R. Soc. Lond. A* **322**, 243–279 (1987).
199. Krupa, M. Bifurcations of relative equilibria. *SIAM J. Math. Anal.* **21**, 1453 (1990).
200. Field, M. J. Equivariant dynamical systems. *Trans. Am. Math. Soc.* **259**, 185 (1980).
201. Toner, J. & Tu, Y. Flocks, herds, and schools: a quantitative theory of flocking. *Phys. Rev. E* **58**, 4828 (1998).
202. Geyer, D., Morin, A. & Bartolo, D. Sounds and hydrodynamics of polar active fluids. *Nat. Mater.* **17**, 789 (2018).
203. Bain, N. & Bartolo, D. Dynamic response and hydrodynamics of polarized crowds. *Science* **363**, 46 (2019).
204. Dean, D. S. Langevin equation for the density of a system of interacting Langevin processes. *J. Phys. Math. Gen.* **29**, L613 (1996).
205. Bertin, E., Droz, M. & Grégoire, G. Boltzmann and hydrodynamic description for self-propelled particles. *Phys. Rev. E* **74**, 022101 (2006).
206. Bertin, E., Droz, M. & Grégoire, G. Hydrodynamic equations for self-propelled particles: microscopic derivation and stability analysis. *J. Phys. A Math. Theor.* **42**, 445001 (2009).

207. Farrell, F. D. C., Marchetti, M. C., Marenduzzo, D. & Tailleur, J. Pattern formation in self-propelled particles with density-dependent motility. *Phys. Rev. Lett.* **108**, 248101 (2012).
208. Chaté, H. & Mahault, B. Dry, aligning, dilute, active matter: a synthetic and self-contained overview. Preprint at https://arxiv.org/abs/1906.05542 (2019).
209. Peshkov, A., Bertin, E., Ginelli, F. & Chaté, H. Boltzmann–Ginzburg–Landau approach for continuous descriptions of generic Vicsek-like models. *Eur. Phys. J. Spec. Top.* **223**, 1315 (2014).
210. Ihle, T. Kinetic theory of flocking: derivation of hydrodynamic equations. *Phys. Rev. E* **83**, 030901 (2011).
211. Mahault, B., Ginelli, F. & Chaté, H. Quantitative assessment of the Toner and Tu theory of polar flocks. *Phys. Rev. Lett.* **123**, 218001 (2019).
212. Oza, A. U. & Dunkel, J. Antipolar ordering of topological defects in active liquid crystals. *New J. Phys.* **18**, 093006 (2016).
213. Suzuki, R., Weber, C. A., Frey, E. & Bausch, A. R. Polar pattern formation in driven filament systems requires non-binary particle collisions. *Nat. Phys.* **11**, 839 (2015).
214. Nishiguchi, D., Nagai, K. H., Chaté, H. & Sano, M. Long-range nematic order and anomalous fluctuations in suspensions of swimming filamentous bacteria. *Phys. Rev. E* **95**, 020601 (2017).
215. Tsai, J.-C., Ye, F., Rodriguez, J., Gollub, J. P. & Lubensky, T. C. A chiral granular gas. *Phys. Rev. Lett.* **94**, 214301 (2005).
216. Liebchen, B. & Levis, D. Collective behavior of chiral active matter: pattern formation and enhanced flocking. *Phys. Rev. Lett.* **119**, 058002 (2017).
217. O'Keeffe, K. P., Hong, H. & Strogatz, S. H. Oscillators that sync and swarm. *Nat. Commun.* **8**, 1504 (2017).
218. Levis, D., Pagonabarraga, I. & Liebchen, B. Activity induced synchronization: mutual flocking and chiral self-sorting. *Phys. Rev. Res.* **1**, 023026 (2019).
219. Burns, K. J., Vasil, G. M., Oishi, J. S., Lecoanet, D. & Brown, B. P. Dedalus: a flexible framework for numerical simulations with spectral methods. *Phys. Rev. Res.* **2**, 023068 (2020).
220. Caussin, J.-B. et al. Emergent spatial structures in flocking models: a dynamical system insight. *Phys. Rev. Lett.* **112**, 148102 (2014).
221. Mishra, S., Baskaran, A. & Marchetti, M. C. Fluctuations and pattern formation in self-propelled particles. *Phys. Rev. E* **81**, 061916 (2010).
222. Grégoire, G. & Chaté, H. Onset of collective and cohesive motion. *Phys. Rev. Lett.* **92**, 025702 (2004).
223. Aditi Simha, R. & Ramaswamy, S. Hydrodynamic fluctuations and instabilities in ordered suspensions of self-propelled particles. *Phys. Rev. Lett.* **89**, 058101 (2002).
224. Kuramoto, Y. *Chemical Oscillations, Waves, and Turbulence* (Springer, 1984).
225. Daido, H. Population dynamics of randomly interacting self-oscillators. I: Tractable models without frustration. *Prog. Theor. Phys.* **77**, 622 (1987).
226. Omata, S., Yamaguchi, Y. & Shimizu, H. Entrainment among coupled limit cycle oscillators with frustration. *Physica D* **31**, 397 (1988).
227. Martens, E. A. et al. Exact results for the Kuramoto model with a bimodal frequency distribution. *Phys. Rev. E* **79**, 026204 (2009).
228. Bonilla, L., Vicente, C. P. & Spigler, R. Time-periodic phases in populations of nonlinearly coupled oscillators with bimodal frequency distributions. *Physica D* **113**, 79 (1998).
229. Hong, H. & Strogatz, S. H. Mean-field behavior in coupled oscillators with attractive and repulsive interactions. *Phys. Rev. E* **85**, 056210 (2012).
230. Ott, E. & Antonsen, T. M. Low dimensional behavior of large systems of globally coupled oscillators. *Chaos* **18**, 037113 (2008).
231. Abrams, D. M., Mirollo, R., Strogatz, S. H. & Wiley, D. A. Solvable model for chimera states of coupled oscillators. *Phys. Rev. Lett.* **101**, 084103 (2008).
232. Pikovsky, A. & Rosenblum, M. Partially integrable dynamics of hierarchical populations of coupled oscillators. *Phys. Rev. Lett.* **101**, 264103 (2008).
233. Martens, E. A., Bick, C. & Panaggio, M. J. Chimera states in two populations with heterogeneous phase-lag. *Chaos* **26**, 094819 (2016).
234. Choe, C.-U., Ri, J.-S. & Kim, R.-S. Incoherent chimera and glassy states in coupled oscillators with frustrated interactions. *Phys. Rev. E* **94**, 032205 (2016).
235. Gallego, R., Montbrió, E. & Pazó, D. Synchronization scenarios in the Winfree model of coupled oscillators. *Phys. Rev. E* **96**, 042208 (2017).
236. Ott, E. & Antonsen, T. M. Long time evolution of phase oscillator systems. *Chaos* **19**, 023117 (2009).
237. Watanabe, S. & Strogatz, S. H. Integrability of a globally coupled oscillator array. *Phys. Rev. Lett.* **70**, 2391 (1993).
238. Watanabe, S. & Strogatz, S. H. Constants of motion for superconducting Josephson arrays. *Physica D* **74**, 197 (1994).
239. Marvel, S. A., Mirollo, R. E. & Strogatz, S. H. Identical phase oscillators with global sinusoidal coupling evolve by Möbius group action. *Chaos* **19**, 043104 (2009).
240. Pikovsky, A. & Rosenblum, M. Dynamics of heterogeneous oscillator ensembles in terms of collective variables. *Physica D* **240**, 872 (2011).
241. Tyulkina, I. V., Goldobin, D. S., Klimenko, L. S. & Pikovsky, A. Dynamics of noisy oscillator populations beyond the Ott–Antonsen ansatz. *Phys. Rev. Lett.* **120**, 264101 (2018).
242. Montbrió, E., Pazó, D. & Roxin, A. Macroscopic description for networks of spiking neurons. *Phys. Rev. X* **5**, 021028 (2015).
243. Bick, C., Goodfellow, M., Laing, C. R. & Martens, E. A. Understanding the dynamics of biological and neural oscillator networks through exact mean-field reductions: a review. *J. Math. Neurosci.* **10**, 9 (2020).
244. Pazó, D. & Montbrió, E. Existence of hysteresis in the Kuramoto model with bimodal frequency distributions. *Phys. Rev. E* **80**, 046215 (2009).
245. Pietras, B., Deschle, N. & Daffertshofer, A. First-order phase transitions in the Kuramoto model with compact bimodal frequency distributions. *Phys. Rev. E* **98**, 062219 (2018).
246. Doppler, J. et al. Dynamically encircling an exceptional point for asymmetric mode switching. *Nature* **537**, 76 (2016).
247. Dembowski, C. et al. Encircling an exceptional point. *Phys. Rev. E* **69**, 056216 (2004).
248. Milburn, T. J. et al. General description of quasiadiabatic dynamical phenomena near exceptional points. *Phys. Rev. A* **92**, 052124 (2015).
249. Mailybaev, A. A., Kirillov, O. N. & Seyranian, A. P. Geometric phase around exceptional points. *Phys. Rev. A* **72**, 014104 (2005).
250. Galda A. & Vinokur, V. M. Parity–time symmetry breaking in magnetic systems. *Phys. Rev. B* **94**, 020408(R) (2016); erratum **100**, 209902 (2019).
251. Galda, A. & Vinokur, V. M. Exceptional points in classical spin dynamics. *Sci. Rep.* **9**, 17484 (2019).
252. Kepesidis, K. V. et al. PT-symmetry breaking in the steady state of microscopic gain–loss systems. *New J. Phys.* **18**, 095003 (2016).
253. Graefe, E.-M., Korsch, H. J. & Niederle, A. E. Quantum–classical correspondence for a non-Hermitian Bose–Hubbard dimer. *Phys. Rev. A* **82**, 013629 (2010).
254. Cartarius, H., Main, J. & Wunner, G. Discovery of exceptional points in the Bose–Einstein condensation of gases with attractive 1/r interaction. *Phys. Rev. A* **77**, 013618 (2008).
255. Gutöhrlein, R., Main, J., Cartarius, H. & Wunner, G. Bifurcations and exceptional points in dipolar Bose–Einstein condensates. *J. Phys. A* **46**, 305001 (2013).
256. Hoyle, R. *Pattern Formation* (Cambridge Univ. Press, 2006).
257. Cross, M. & Greenside, H. *Pattern Formation and Dynamics in Nonequilibrium Systems* (Cambridge Univ. Press, 2009).
258. Meron, E. *Nonlinear Physics of Ecosystems* (CRC Press, 2015).
259. Swift, J. & Hohenberg, P. C. Hydrodynamic fluctuations at the convective instability. *Phys. Rev. A* **15**, 319 (1977).
260. Coullet, P. & Fauve, S. Propagative phase dynamics for systems with galilean invariance. *Phys. Rev. Lett.* **55**, 2857 (1985).
261. Brachet, M. E., Coullet, P. & Fauve, S. Propagative phase dynamics in temporally intermittent systems. *Europhys. Lett.* **4**, 1017 (1987).
262. Douady, S., Fauve, S. & Thual, O. Oscillatory phase modulation of parametrically forced surface waves. *Europhys. Lett.* **10**, 309 (1989).
263. Coullet, P. & looss, G. Instabilities of one-dimensional cellular patterns. *Phys. Rev. Lett.* **64**, 866 (1990).
264. Fauve, S., Douady, S. & Thual, O. Drift instabilities of cellular patterns. *J. Phys. II* **1**, 311 (1991).
265. Knobloch, E., Hettel, J. & Dangelmayr, G. Parity-breaking bifurcation in inhomogeneous systems. *Phys. Rev. Lett.* **74**, 4839 (1995).
266. Armbruster, D., Guckenheimer, J. & Holmes, P. Heteroclinic cycles and modulated travelling waves in systems with O(2) symmetry. *Physica D* **29**, 257 (1988).
267. Proctor, M. R. E. & Jones, C. A. The interaction of two spatially resonant patterns in thermal convection. Part 1. Exact 1:2 resonance. *J. Fluid Mech.* **188**, 301 (1988).
268. Dangelmayr, G., Hettel, J. & Knobloch, E. Parity-breaking bifurcation in inhomogeneous systems. *Nonlinearity* **10**, 1093 (1997).
269. Simon, A. J., Bechhoefer, J. & Libchaber, A. Solitary modes and the Eckhaus instability in directional solidification. *Phys. Rev. Lett.* **61**, 2574 (1988).
270. Flesselles, J.-M., Simon, A. & Libchaber, A. Dynamics of one-dimensional interfaces: an experimentalist's view. *Adv. Phys.* **40**, 1 (1991).
271. Melo, F. & Oswald, P. Destabilization of a faceted smectic-A–smectic-B interface. *Phys. Rev. Lett.* **64**, 1381 (1990).
272. Faivre, G. & Mergy, J. Dynamical wavelength selection by tilt domains in thin-film lamellar eutectic growth. *Phys. Rev. A* **46**, 963 (1992).
273. Kassner, K. & Misbah, C. Parity breaking in eutectic growth. *Phys. Rev. Lett.* **65**, 1458–1461 (1990).
274. Ginibre, M., Akamatsu, S. & Faivre, G. Experimental determination of the stability diagram of a lamellar eutectic growth front. *Phys. Rev. E* **56**, 780–796 (1997).
275. Cummins, H. Z., Fourtune, L. & Rabaud, M. Successive bifurcations in directional viscous fingering. *Phys. Rev. E* **47**, 1727–1738 (1993).
276. Bellon, L., Fourtune, L., Minassian, V. T. & Rabaud, M. Wave-number selection and parity-breaking bifurcation in directional viscous fingering. *Phys. Rev. E* **58**, 565–574 (1998).
277. Counillon, C. et al. Global drift of a circular array of liquid columns. *Europhys. Lett.* **40**, 37 (1997).
278. Knobloch, E. & Proctor, M. R. E. Nonlinear periodic convection in double-diffusive systems. *J. Fluid Mech.* **108**, 291–316 (1981).
279. Cross, M. C. & Kim, K. Linear instability and the codimension-2 region in binary fluid convection between rigid impermeable boundaries. *Phys. Rev. A* **37**, 3909–3920 (1988).
280. Cross, M. C. Traveling and standing waves in binary-fluid convection in finite geometries. *Phys. Rev. Lett.* **57**, 2935–2938 (1986).
281. Coullet, P. H. & Spiegel, E. A. Amplitude equations for systems with competing instabilities. *SIAM J. Appl. Math.* **43**, 776–821 (1983).
282. Cross, M. C. Structure of nonlinear traveling-wave states in finite geometries. *Phys. Rev. A* **38**, 3593–3600 (1988).
283. Brand, H. R., Hohenberg, P. C. & Steinberg, V. Amplitude equation near a polycritical point for the convective instability of a binary fluid mixture in a porous medium. *Phys. Rev. A* **27**, 591–593 (1983).
284. Brand, H. R., Hohenberg, P. C. & Steinberg, V. Codimension-2 bifurcations for convection in binary fluid mixtures. *Phys. Rev. A* **30**, 2548–2561 (1984).
285. Guckenheimer, J. Multiple bifurcation problems of codimension two. *SIAM J. Math. Anal.* **15**, 1–49 (1984).
286. Moses, E. & Steinberg, V. Flow patterns and nonlinear behavior of traveling waves in a convective binary fluid. *Phys. Rev. A* **34**, 693–696 (1986); erratum **35**, 1444–1445 (1987).
287. Walden, R. W., Kolodner, P., Passner, A. & Surko, C. M. Traveling waves and chaos in convection in binary fluid mixtures. *Phys. Rev. Lett.* **55**, 496–499 (1985).
288. Coullet, P., Fauve, S. & Tirapegui, E. Large scale instability of nonlinear standing waves. *J. Physique Lett.* **46**, 787–791 (1985).
289. Bensimon, D., Pumir, A. & Shraiman, B. Nonlinear theory of traveling wave convection in binary mixtures. *J. Phys. France* **50**, 3089–3108 (1989).
290. Knobloch, E. & Moore, D. R. Minimal model of binary fluid convection. *Phys. Rev. A* **42**, 4693–4709 (1990).
291. Schöpf, W. & Zimmermann, W. Convection in binary fluids: amplitude equations, codimension-2 bifurcation, and thermal fluctuations. *Phys. Rev. E* **47**, 1739–1764 (1993).

292. Bressloff, P. C., Cowan, J. D., Golubitsky, M., Thomas, P. J. & Wiener, M. C. Geometric visual hallucinations, Euclidean symmetry and the functional architecture of striate cortex. *Phil. Trans. R. Soc. Lond. B* **356**, 299–330 (2001).
293. Bressloff, P. C., Cowan, J. D., Golubitsky, M., Thomas, P. J. & Wiener, M. C. What geometric visual hallucinations tell us about the visual cortex. *Neural Comput*. **14**, 473–491 (2002).
294. Cho, M. W. & Kim, S. Understanding visual map formation through vortex dynamics of spin Hamiltonian models. *Phys. Rev. Lett*. **92**, 018101 (2004).
295. Schnabel, M., Kaschube, M. & Wolf, F. Pinwheel stability, pattern selection and the geometry of visual space. Preprint at https://arxiv.org/abs/0801.3832 (2008).
296. Butler, T. C. et al. Evolutionary constraints on visual cortex architecture from the dynamics of hallucinations. *Proc. Natl Acad. Sci. USA* **109**, 606–609 (2012).
297. Curtu, R. & Ermentrout, B. Pattern formation in a network of excitatory and inhibitory cells with adaptation. *SIAM J. Appl. Dyn. Syst*. **3**, 191–231 (2004).
298. Adini, Y., Sagi, D. & Tsodyks, M. Excitatory–inhibitory network in the visual cortex: psychophysical evidence. *Proc. Natl Acad. Sci. USA* **94**, 10426–10431 (1997).
299. Hensch, T. K. & Fagiolini, M. in *Progress in Brain Research* (eds van Pelt, J. et al.) 115–124 (Elsevier, 2005).
300. Chossat, P. & Iooss, G. *The Couette–Taylor Problem* (Springer, 1994).
301. Riecke, H. & Paap, H.-G. Parity-breaking and Hopf bifurcations in axisymmetric Taylor vortex flow. *Phys. Rev. A* **45**, 8605–8610 (1992).
302. Tennakoon, S. G. K., Andereck, C. D., Hegseth, J. J. & Riecke, H. Temporal modulation of traveling waves in the flow between rotating cylinders with broken azimuthal symmetry. *Phys. Rev. E* **54**, 5053–5065 (1996).
303. Mutabazi, I. & Andereck, C. D. Mode resonance and wavelength-halving instability in the Taylor–Dean system. *Phys. Rev. E* **51**, 4380–4390 (1995).
304. Bot, P., Cadot, O. & Mutabazi, I. Secondary instability mode of a roll pattern and transition to spatiotemporal chaos in the Taylor–Dean system. *Phys. Rev. E* **58**, 3089–3097 (1998).
305. Wiener, R. J. & McAlister, D. F. Parity breaking and solitary waves in axisymmetric Taylor vortex flow. *Phys. Rev. Lett*. **69**, 2915–2918 (1992).
306. Andereck, C. D., Liu, S. S. & Swinney, H. L. Flow regimes in a circular Couette system with independently rotating cylinders. *J. Fluid Mech*. **164**, 155–183 (1986).
307. Altmeyer, S. & Hoffmann, C. Secondary bifurcation of mixed-cross-spirals connecting travelling wave solutions. *New J. Phys*. **12**, 113035 (2010).
308. Pinter, A., Lücke, M. & Hoffmann, C. Competition between traveling fluid waves of left and right spiral vortices and their different amplitude combinations. *Phys. Rev. Lett*. **96**, 044506 (2006).
309. Hong, H. Periodic synchronization and chimera in conformist and contrarian oscillators. *Phys. Rev. E* **89**, 062924 (2014).
310. Kemeth, F. P., Haugland, S. W., Schmidt, L., Kevrekidis, I. G. & Krischer, K. A classification scheme for chimera states. *Chaos* **26**, 094815 (2016).
311. Golubitsky, M. & Stewart, I. Hopf bifurcation in the presence of symmetry. *Arch. Ration. Mech. Anal*. **87**, 107–165 (1985).
312. Shapere, A. & Wilczek, F. Classical time crystals. *Phys. Rev. Lett*. **109**, 160402 (2012).
313. Wilczek, F. Quantum time crystals. *Phys. Rev. Lett*. **109**, 160401 (2012).
314. Yao, N. Y. & Nayak, C. Time crystals in periodically driven systems. *Phys. Today* **71**, 40 (2018).
315. Prigogine, I. & Lefever, R. Symmetry-breaking instabilities in dissipative systems. *II. J. Chem. Phys*. **48**, 1695–1700 (1968).
316. Giergiel, K., Miroszewski, A. & Sacha, K. Time crystal platform: from quasicrystal structures in time to systems with exotic interactions. *Phys. Rev. Lett*. **120**, 140401 (2018).
317. Autti, S., Eltsov, V. & Volovik, G. Observation of a time quasicrystal and its transition to a superfluid time crystal. *Phys. Rev. Lett*. **120**, 215301 (2018).

Acknowledgements We thank A. Alù, D. Bartolo, D. Christodoulides, A. Clerk, A. Edelman, A. Galda, M. Han, K. Husain, T. Kottos, Z. Lu, M. C. Marchetti, M.-A. Miri, B. Roussel, C. Scheibner, D. Schuster, J. Simon and B. van Zuiden. M.F. acknowledges support from a MRSEC-funded Kadanoff–Rice fellowship (DMR-2011854) and the Simons Foundation. R.H. was supported by a Grand-in-Aid for JSPS fellows (grant number 17J01238). V.V. was supported by the Complex Dynamics and Systems Program of the Army Research Office under grant number W911NF-19-1-0268 and the Simons Foundation. This work was partially supported by the University of Chicago Materials Research Science and Engineering Center, which is funded by National Science Foundation under award number DMR-2011854. This work was completed in part with resources provided by the University of Chicago's Research Computing Center. Some of us benefited from participation in the KITP programme on Symmetry, Thermodynamics and Topology in Active Matter supported by grant number NSF PHY-1748958.

Author contributions M.F., R.H., P.B.L. and V.V. designed the research, performed the research, and wrote the paper.

Competing interests The authors declare no competing interests.

Additional information

Supplementary information The online version contains supplementary material available at https://doi.org/10.1038/s41586-021-03375-9.

Correspondence and requests for materials should be addressed to V.V.

Peer review information *Nature* thanks the anonymous reviewers for their contribution to the peer review of this work.

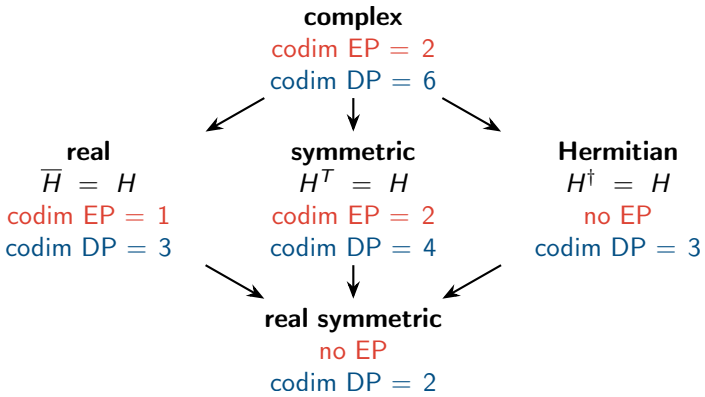

Extended Data Fig. 1 | Codimensions of eigenvalue degeneracies. This graph gives the codimension (codim) of twofold degeneracies of eigenvalues in different matrix spaces; see ref. [194]. These degeneracies can be exceptional points (EP) or diabolic points (DP, also known as Dirac points). An identical graph can be drawn by replacing 'real symmetric' with 'purely imaginary symmetric', 'Hermitian' with 'anti-Hermitian' and 'real' with 'imaginary'.

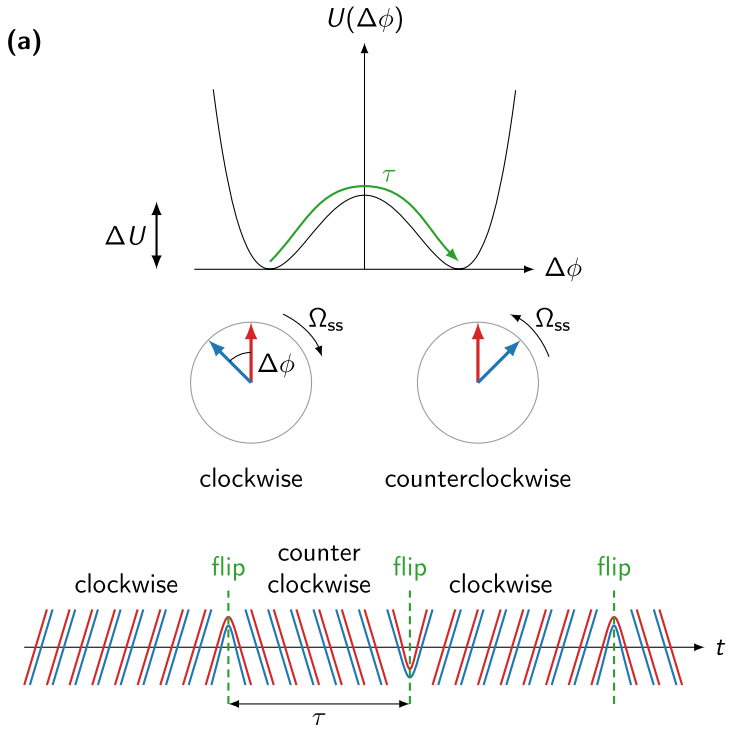

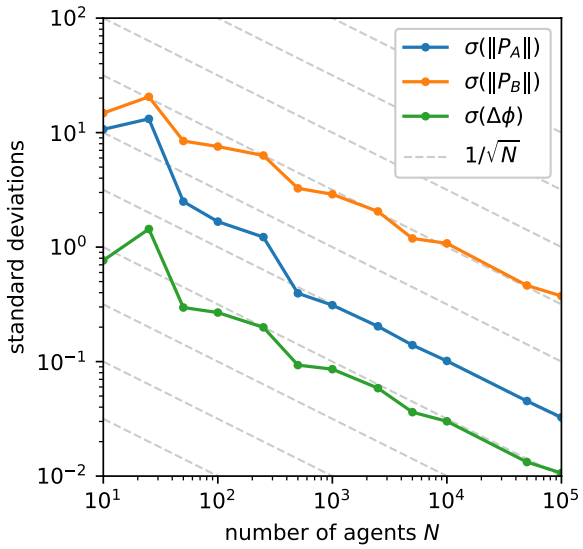

Extended Data Fig. 2 | Many-body suppression of noise-activated chirality inversions. a, A change in the sign of the angle $\Delta\phi$ between the order parameters $\mathbf{v}_A$ and $\mathbf{v}_B$ (in blue and red) flips the chirality (clockwise or anticlockwise) of the chiral phase. Qualitatively, the two steady-state values $\pm\Delta\phi_c$ towards which the system relax correspond to the minima of an effective potential $U(\Delta\phi)$, with a barrier ΔU separating these minima. The lifetime of the chiral phase is the average time τ separating two flips of chirality (represented in green), namely the Kramers escape time required to jump from one minimum to the other under the effect of noise. **b**, The standard deviations quantifying the fluctuations of the order parameters $\mathbf{v}_a$ in the chiral phase decrease approximately as $1/\sqrt{N}$ with the number of agents N. The grey lines are equally spaced $1/\sqrt{N}$ curves and are meant as a guide to the eye (not a fit). The data are obtained from simulations of the Kuramoto model equation (2) with $J_{AA}=J_{BB}=1$, $J_{AB}=1$, $J_{BA}=-1.1$, $\eta=8\times10^{-2}$ and all-to-all couplings. The total duration is $T_{sim}/\delta t=4{,}000$ with $\delta t=0.5$, over which the standard deviation is computed.

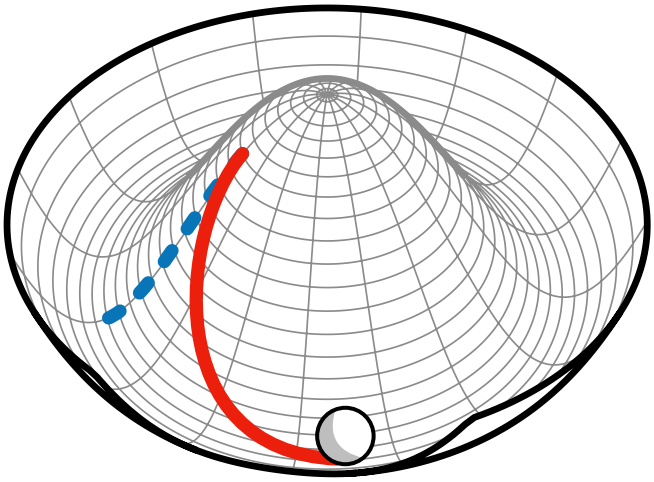

Extended Data Fig. 3 | Effect of non-conservative forces. In this simplified pictorial representation, the order parameter (represented by a ball) evolves in a potential-energy landscape shaped like a sombrero. In a conservative system, the order parameter would relax straight to the bottom of the potential (dashed blue line). Here, transverse non-conservative forces push the order parameter in the direction defined by the bottom of the potential, leading to a curved trajectory (red continuous line) starting from the same initial condition. In the systems we considered, the non-conservative forces arise from the non-reciprocal coupling between two order parameters. This aspect is not captured by this simplified picture.

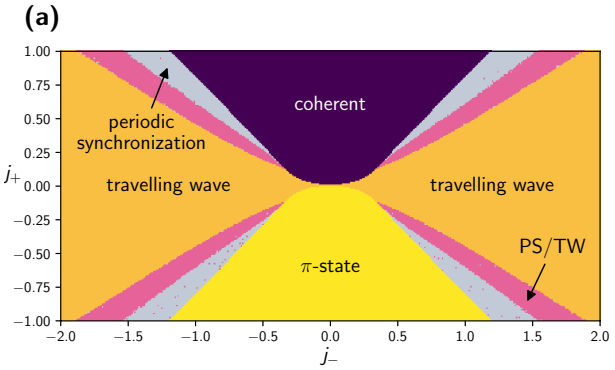

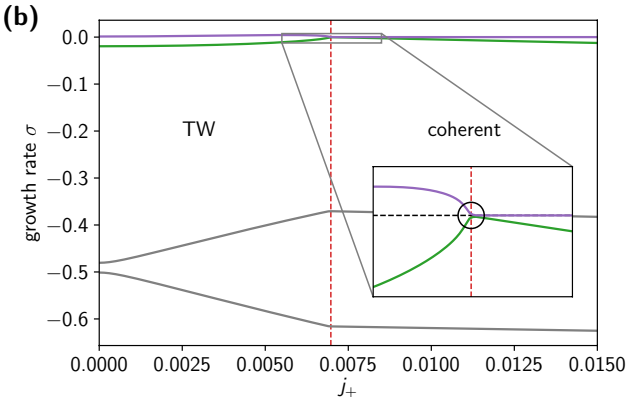

Extended Data Fig. 4 | Phase diagram of the PT-symmetric non-reciprocal Kuramoto model and exceptional point in the spectrum of the Jacobian. **a**, Phase diagram computed numerically from equation (15). The states are defined in Extended Data Table 1. **b**, The two most unstable eigenvalues $\lambda_i = \sigma_i + i\omega_i$ of L coalesce at $j_+ \approx 0.007$. This value coincides with the transition from travelling waves (TW) to coherent states, marked by a red dashed line. Note that this coalescence occurs at $\lambda = 0$ (not at finite frequency nor at finite growth rate). The corresponding eigenvectors become collinear (this can be verified, for instance, by computing the determinant of the matrix of eigenvectors, that vanishes at the exceptional point). The imaginary parts ω_i (not shown) are all zero. We have set $j_{AA} = j_{BB} = 1$, $\Delta_A = \Delta_B = 0.25$ and $\omega_A = \omega_B = 0$. In **b**, $j_- = 0.1$ (a similar behaviour is observed for neighbouring values of j_-).

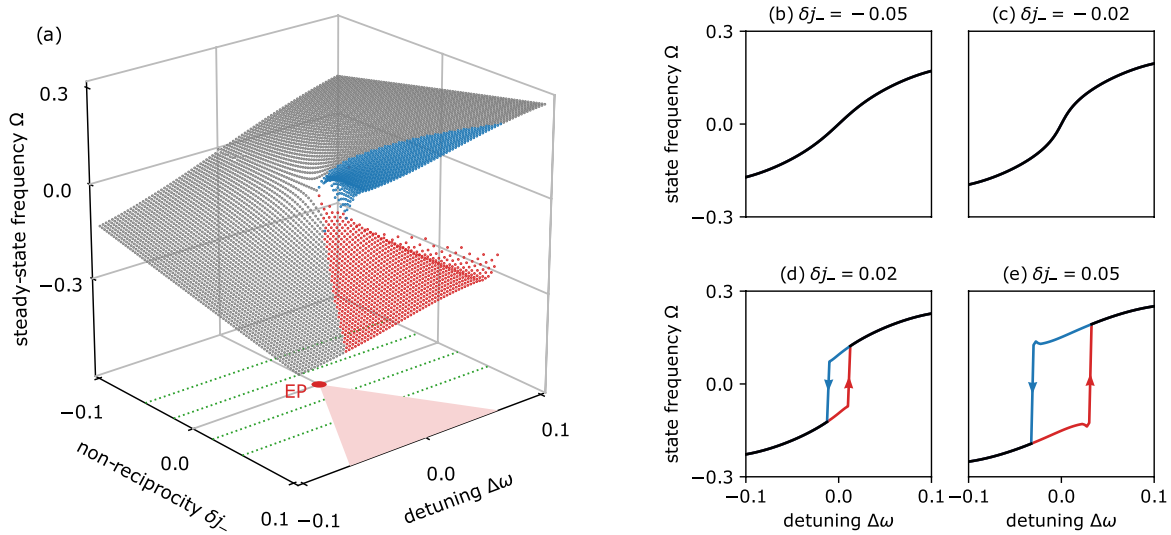

Extended Data Fig. 5 | Hysteresis in the chiral Kuramoto model. When chirality is explicitly broken, exceptional points have codimension two, that is, they are typically points in a two-dimensional parameter space. **a**, We plot the frequency Ω of the steady state of the Kuramoto model with explicitly broken PT symmetry as a function of the difference $\Delta\omega = \omega_A - \omega_B$ between the two communities (also called detuning) and the deviation $\delta j_- = j_- - j_-^{EP}$ of the non-reciprocal part j_- of the coupling between the communities from its value j_-^{EP} at the exceptional point. The system exhibits a region where two possible steady states with different properties coexist (the two steady states are the continuation of the clockwise and anticlockwise chiral phases present in the PT-symmetric case $\Delta\omega = 0$). This region (red triangle) starts at the exceptional point (red point) and its size increases with the amount of non-reciprocity (here $j_-^{EP} \approx 0.2915 > 0$). The system exhibits hysteresis in the coexistence region (red points). **b**–**e**, Slices from **a** at fixed δj_- (marked by green dotted lines in **a**). After the exceptional point, there is hysteresis/first-order (discontinuous) behaviour. In **d**, the hysteresis curve bends outwards near the transition. This is due to the oscillation of the norm of the order parameter (which we refer to as swap or periodic synchronization elsewhere) for large enough δj_-. This additional complication does not occur for moderate values of δj_-, such as in **c**. The solution of the dynamical system equation (15) were computed along lines at fixed δj_-, starting at large $|\delta\omega|$ (in a region without phase coexistence) from a random initial condition. The solution (after convergence) was used as an initial value for the next point in the line with fixed δj_-. This procedure was carried out two times, starting from positive and negative large $|\delta\omega|$. We have set $j_+ = 0.08$, $j_{AA} = j_{BB} = 1$, $\Delta_A = \Delta_B = 0.25$, $\omega_A = \omega_B = \Delta\omega/2$.

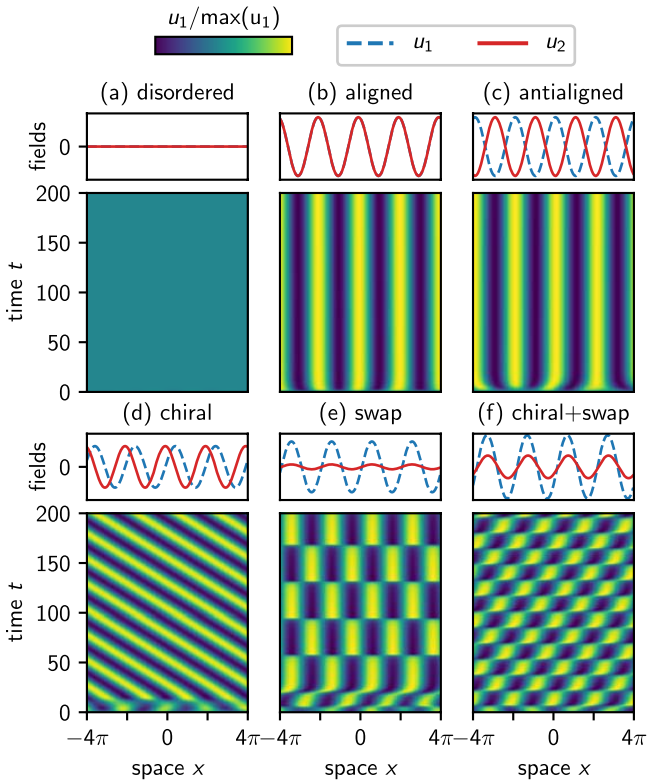

Extended Data Fig. 6 | Non-reciprocal pattern formation. We show a space-time density plot of the field $u_1(x, t)$ in different phases, as well as snapshots of the fields $u_1(x, t)$ and $u_2(x, t)$ at time $t = 200$. **a**, We observe a disordered phase where both field vanish. **b**, An aligned phase where both patterns are static and in phase (superimposed). **c**, An antialigned phase where the patterns are static and completely out of phase. **d**, A chiral phase where the patterns move at constant velocity, either to the left or to the right (spontaneously breaking parity), and in which the fields have a finite phase difference, usually neither zero nor π. **e**, A swap phase where the patterns essentially jump by a phase π every period. **f**, A mix of the chiral and swap behaviours (as in the chiral phase (**d**), there is a spontaneously broken symmetry between left and right movers). The fields are obtained by direct numerical simulation of the coupled Swift–Hohenberg equations on a one-dimensional domain of size $2L$ with periodic boundary conditions, starting from random initial conditions. The simulations are performed using the open-source pseudospectral solver Dedalus[219]. We have used $g = 0.25$ in all cases. In **a**, $r_{11} = r_{22} = -0.5$ and $r_+ = r_- = 0.00$. In the other cases, we have set $r_{11} = r_{22} = 0.5$ (**b**–**f**) and $r_+ = 0.50, r_- = 0.00$ (**b**); $r_+ = -0.50, r_- = 0.00$ (**c**); $r_+ = 0.00, r_- = 0.25$ (**d**); $r_+ = 0.87, r_- = 1.00$ (**e**); $r_+ = 0.85, r_- = 1.00$ (**f**).

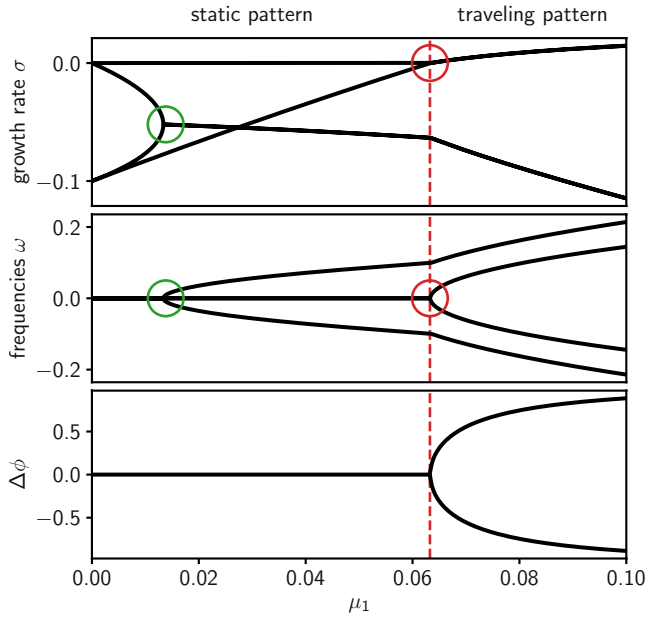

Extended Data Fig. 7 | Exceptional point in directional interface growth. The spectrum of the Jacobian L corresponding to equation (20) exhibits an exceptional point at the transition between static patterns and travelling patterns with spontaneous parity breaking (that is, the patterns travel with equal probability to the left or to the right). The two most unstable eigenvalues $\lambda_i = \sigma_i + i\omega_i$ of L coalesce at $\mu_1 \approx 0.064$ (red circle). This value coincides with the transition from a constant solution to travelling waves, marked by a red dashed line. The coalescence occurs at $\lambda = 0$ (not at finite frequency nor at finite growth rate), and the corresponding eigenvectors become collinear. Note that another exceptional point occurs near $\mu_1 \approx 0.014$ (green circle), but with a strictly negative growth rate: this does not correspond to a bifurcation. We also show the dephasing $\Delta\phi = 2\phi_1 - \phi_2$ between the amplitudes, which undergoes a pitchfork bifurcation; the direction of motion of the pattern is set by $\Delta\phi$. We have set $\alpha = \beta = \gamma = \delta = 1$, $\varepsilon = +1$ and $\mu_2 = -0.1$.

Extended Data Table 1 | An O(2) 'Rosetta stone'

state	**flocking**	**synchronization**	**patterns**	r_a	$\phi_B - \phi_A$
trivial	disordered	incoherent	none	0	n/a
aligned	flocking	coherent	in-phase	constant $\neq 0$	0
antialigned	antiflocking	π-state	anti-phase	constant $\neq 0$	π
chiral	chiral	traveling wave state	traveling	constant $\neq 0$	constant $\neq 0, \pi$
swap	swap	periodic synchronization	modulated	time-dependent	constant mod π
swap+chiral	swap+chiral	PS+TW	traveling modulated	time-dependent	time-dependent

Definitions of the states in the different systems. The complex order parameters $z_a = r_a e^{i\phi}$ are decomposed in amplitude $r_a = |z_a|$ and phase $e^{i\phi_a} = z_a/|z_a|$. The label 'PS+TW' corresponds to 'periodic synchronization + traveling wave'. For synchronization, we mostly followed the nomenclature of refs. [12,33,135,229,234,309,310] and we do not distinguish fully coherent states ($r = 1$) from partially coherent ones ($0 \neq r < 1$), both are called 'coherent'. These different states can be understood from symmetries; see refs. [22,68,69,199,200,311]. The chiral, swap and swap+chiral states/phases break time-translation invariance in a way reminiscent of time crystals[53,54,312–315] and quasicrystals[316,317], as illustrated in Supplementary Video 2.